Contribution from the Department of Chemistry and Biochemistry, University of Maryland, College Park, Maryland 20742

Mononuclear Octahedral and Dinuclear Edge-Sharing and Face-Sharing Bioctahedral Compounds of Molybdenum(III). Electronic Control on the Extent of Metal-Metal Interaction in the Dinuclear Systems. An Equilibrium, Structural, and Paramagnetic NMR Study

Rinaldo Poli* and Humberto D. Mui

Received June 28, 1990

Octahedral Mo(III) mononuclear and edge-sharing and face-sharing dinuclear complexes have been investigated. The ^{1}H NMR spectra of mononuclear compounds of formula MoX_3L_3 (X = Cl, Br, I; L = PMe_3, PEt_3, PMe_2Ph) establishes their meridional configuration in solution. The temperature dependence of the spectra is consistent with Curie behavior. The face-sharing bioctahedral complexes $Mo_2Cl_6L_3$ (L = PEt_3, PMe_2Ph) react with free phosphine to afford the corresponding edge-sharing bioctahedral complexes $Mo_2Cl_6L_4$, which in turn react with more phosphine to produce the mononuclear $MoCl_3L_3$ complexes. The edge-sharing complexes slowly disproportionate to mixtures of the face-sharing dimers and monomers. The relative stability of the complexes in a phosphine-rich environment is as follows: face-sharing < edge-sharing ≪ monomer. The $Mo_2Cl_6(PMe_2Ph)_4$ compound has been crystallographically characterized. It shows the same edge-sharing bioctahedral geometry but a dramatically different metal-metal separation (2.8036 (8) Å) with respect to that of the $Mo_2Cl_6(PEt_3)_4$ molecule reported earlier. Possible causes for this difference are discussed. Crystal data for $Mo_2Cl_6(PMe_2Ph)_4 \cdot 2CHCl_3$: triclinic, space group $P\bar{1}$, a = 10.618 (3) Å, b = 13.297 (3) Å, c = 18.823 (4) Å, α = 73.96 (2)°, β = 86.16 (1)°, γ = 77.13 (2)°, V = 2490 (2) Å^3, Z = 2, d_c = 1.60 g·cm^{-3}, μ(Mo Kα) = 12.88 cm^{-1}, R = 0.034 (R_w = 0.047) for 469 parameters and 6076 unique data with $F_o^2 > 3\sigma(F_o^2)$. The ^{1}H NMR properties of this compound and of $Mo_2Cl_6(PEt_3)_4$ have been investigated at variable temperature. While the PMe_2Ph complex shows only small paramagnetic shifts with a temperature-dependence consistent with a diamagnetic ground state and a slightly populated paramagnetic excited state, the PEt_3 complex shows large paramagnetic shifts and a temperature dependence similar to that exhibited by the mononuclear compounds. The $Mo_2Cl_6L_3$ (L = PEt_3, PMe_2Ph) complexes have also been structurally characterized. Crystal data for $Mo_2Cl_6(PMe_2Ph)_3$: triclinic, space group $P\bar{1}$, a = 9.769 (1) Å, b = 12.9813 (6) Å, c = 13.744 (2) Å, α = 76.299 (6)°, β = 82.16 (1)°, γ = 71.682 (2)°, V = 1603.9 (5) Å^3, Z = 2, d_c = 1.70 g·cm^{-3}, μ(Cu Kα) = 128.07 cm^{-1}, R = 0.038 (R_w = 0.061) for 316 parameters and 3716 unique data with $F_o^2 > 3\sigma(F_o^2)$. Crystal data for $Mo_2Cl_6(PEt_3)_3 \cdot CH_2Cl_2$: monoclinic, space group $P2_1/n$, a = 14.212 (2) Å, b = 13.146 (3) Å, c = 19.090 (4) Å, β = 99.61 (1)°, V = 3516 (2) Å^3, Z = 4, d_c = 1.59 g·cm^{-3}, μ(Cu Kα) = 130.51 cm^{-1}, R = 0.080 (R_w = 0.099) for 289 parameters and 2928 unique data with $F_o^2 > 3\sigma(F_o^2)$. Both structures show the metal-metal-bonded Mo_2 core at the center of a face-sharing bioctahedral arrangement of the ligands in a relative anti configuration. The metal-metal distance is 2.753 (2) Å (PEt_3) and 2.6582 (5) Å (PMe_2Ph), respectively, indicating strong bonding. Both compounds exist as equilibrium mixtures of anti and gauche isomers in solution and exhibit slight paramagnetic shifts in the ^{1}H NMR spectra with a temperature dependence similar to that of $Mo_2Cl_6(PMe_2Ph)_4$.

Introduction

The relative strength of metal-ligand and metal-metal bonds brings contrasting properties to transition-metal compounds.[1] Maximizing metal-ligand bonding is usually the choice for first transition elements whereas metal-metal bonding becomes increasingly important for the heavier elements, so that complexes of 3d elements are typically mononuclear whereas oligonuclear, metal-metal-bonded complexes with lower coordination numbers are often found for 5d elements.

Group 6 metals seem to provide the most striking examples. For instance, $Cr_2Cl_4(L\text{-}L)_2$ (L-L = bidentate phosphine) compounds have a halide-bridged, non-metal-metal-bonded structure, $(L\text{-}L)ClCr(\mu\text{-}Cl)_2CrCl(L\text{-}L)$,[2] where the metal is surrounded by five ligands whereas the molybdenum and tungsten analogues have a non-halide-bridged, quadruply metal-metal-bonded structure, $(L\text{-}L)Cl_2M\overset{4}{-}MCl_2(L\text{-}L)$[3] or $Cl_2M(\mu^2\text{-}L\text{-}L)_2MCl_2$ ($M\overset{4}{-}M$)[4] with only four ligands around each metal center. The series of $M_2Cp_2Cl_4$ (Cp = η^5-C_5H_5) compounds and derivatives is also notable: $Cr_2Cp_2Cl_4$ has a chloride-bridged, non-metal-metal-bonded structure, $CpClCr(\mu\text{-}Cl)_2CrClCp$;[5] $Mo_2Cp'_2Cl_4$ (Cp' = η^6-*i*-PrC_5H_4) has a quadruply bridged, singly metal-metal-bonded structure, $Cp'Mo(\mu\text{-}Cl)_4MoCp'$ (Mo-Mo);[6] and finally the tungsten analogue has a non-bridged, triply metal-metal-bonded structure, $Cp'Cl_2W{\equiv}WCl_2Cp'$.[7] Yet another example is the ionic structure of $CrCl_2$ (the metal coordination number is 6), compared to $MoCl_2$ and WCl_2, which are based on the $[M_6Cl_8]^{4+}$ cluster unit with each metal atom being bonded to only five chloride ligands.[8]

Molybdenum experiences a delicate balance between different forces. For instance, mononuclear compounds of formula MoX_2L_4, formally L adducts of the quadruply bonded $Mo_2X_4L_4$ dimers, represent an extensive class of stable derivatives,[9] whereas only a few tungsten analogues appear to have been described.[10]

In this paper, we are concerned with complexes of molybdenum(III) halides with phosphine ligands. This study had impetus from our recent discovery that the edge-sharing bioctahedral complex $Mo_2Cl_6(PEt_3)_4$ does not exhibit a direct metal-metal bond,[11] whereas all the isostructural $Mo_2X_6(L\text{-}L)_2$ (L-L = diphosphine or disulfide) derivatives reported until then have a short metal-metal separation corresponding to a strong Mo-Mo bond.[12]

(1) Connors, J. A. *Top. Curr. Chem.* **1977**, *71*, 71.
(2) Hermes, A. R.; Girolami, G. S. *Inorg. Chem.* **1988**, *27*, 1775. (b) Cotton, F. A.; Luck, R. L.; Son, K.-A. *Inorg. Chim. Acta* **1990**, *168*, 3.
(3) (a) San Filippo, J., Jr.; Sniadoch, H. J.; Grayson, R. L. *Inorg. Chem.* **1974**, *13*, 2121. (b) Best, S. A.; Smith, T. J.; Walton, R. A. *Inorg. Chem.* **1978**, *17*, 99. (c) Cotton, F. A.; Felthouse, T. R.; Lay, D. G. *J. Am. Chem. Soc.* **1980**, *102*, 1431. (d) Cotton, F. A.; Extine, M. W.; Felthouse, T. R.; Kolthammer, B. W. S.; Lay, D. G. *J. Am. Chem. Soc.* **1981**, *103*, 4040.
(4) (a) Campbell, F. L., III; Cotton, F. A.; Powell, G. L. *Inorg. Chem.* **1985**, *24*, 4384 and references therein. (b) Fryzuk, M. D.; Kreiter, C. G.; Sheldrick, W. S. *Chem. Ber.* **1989**, *122*, 851. See also ref 3c.
(5) Köhler, F. H.; de Cao, R.; Ackermann, K.; Sedlmair, J. *Z. Naturforsch.* **1983**, *38B*, 1406.
(6) Grebenik, P. D.; Green, M. L. H.; Izquierdo, A.; Mtetwa, V. S. B.; Prout, K. *J. Chem. Soc., Dalton Trans.* **1987**, 9.
(7) Green, M. L. H.; Mountford, P. *J. Chem. Soc., Chem. Commun.* **1989**, 732.
(8) Cotton, F. A.; Wilkinson, G. *Advanced Inorganic Chemistry*, 5th ed.; Wiley: New York, 1988; p 846.
(9) Wilkinson, G., Gillard, R. D., McCleverty, J. A., Eds. *Comprehensive Coordination Chemistry*; Pergamon: Oxford, England, 1987; Vol. 3, p 1283-7.
(10) (a) Djordjevic, C.; Nyholm, R. S.; Pande, C. S.; Stiddard, M. H. B. *J. Chem. Soc. A* **1966**, 16. (b) Bell, B.; Chatt, J.; Leigh, G. J. *J. Chem. Soc., Dalton Trans.* **1972**, 2492. (c) Sharp, P. R.; Schrock, R. R. *J. Am. Chem. Soc.* **1980**, *102*, 1430. (d) Sharp, P. R. *Organometallics* **1984**, *3*, 1217.
(11) Mui, H. D.; Poli, R. *Inorg. Chem.* **1989**, *28*, 3609.

0020-1669/91/1330-0065$02.50/0

A key feature for the success of this investigations was the discovery that spin quartet octahedral Mo^{3+} complexes are suitable for ^1H NMR investigations, which also allowed the behavior of these compounds to be investigated *in solution* for the first time. We shall show here that, in addition to metal–ligand and metal–metal bond strengths, one has to consider the role played by electronic correlation effects when dealing with a system in an open-shell electronic configuration.

Experimental Section

All operations were carried out under a dinitrogen atmosphere with carefully dried and distilled solvents by using standard Schlenk line techniques.[13] Instruments used were as follows: FTIR, Nicolet 5DXC; NMR, Bruker WP200 or AF200; magnetic susceptibility balance, Johnson Matthey; UV/vis, Shimadzu UV-240. Elemental analyses were by Midwest Microlab, Indianapolis, IN.

$MoX_3(THF)_3$ (X = Cl,[14] Br,[15] I[16]), $MoX_3(PMe_3)_3$ (X = Cl,[17] I[16]), $MoCl_3(PMe_2Ph)_2(THF)$, $MoCl_3(PMe_2Ph)_3$,[14] and $Mo_2Cl_6(PEt_3)_4$[11] were prepared according to procedures described in the literature. $MoBr_3(PMe_3)_3$, $MoBr_3(PMe_2Ph)_3$, and $MoI_3(PMe_2Ph)_3$ were prepared by adaptations of the syntheses utilized to prepare the analogous chloride compounds. PEt_3 and PMe_2Ph (Strem) were distilled prior to use.

All reactions carried out with NMR monitoring were performed directly in thin-walled 5-mm NMR tubes. For the disproportionation reactions, the transition-metal complexes were introduced directly into the NMR tubes and the solvent was introduced while the tube was kept at 77 K. For the reactions with free phosphine, the solution was prepared at room temperature, transferred into the NMR tube, and then frozen at 77 K and the phosphine introduced with a microsyringe. In each case, the NMR tube was sealed under vacuum and was thawed immediately preceding the introduction into the NMR probe. A control experiment shows that neither PMe_2Ph nor PEt_3 reacts appreciably with $CDCl_3$ during the time scale of our studies, whereas only the former phosphine does not react with CD_2Cl_2.[18]

Preparation of $Mo_2Cl_6(PMe_2Ph)_3$. To a suspension of $MoCl_3(THF)_3$ (1.678 g, 4.008 mmol) in 30 mL of toluene was added 860 μL of PMe_2Ph (6.04 mmol). The mixture was refluxed for 20 h, producing a suspension of the brown microcrystalline product. After the suspension was cooled to room temperature, the product was filtered, washed twice with 5 mL of *n*-heptane, and dried in vacuo. Yield: 1.099 g (67%). Anal. Calcd. for $C_{24}H_{33}Cl_6Mo_2P_3$: C, 35.20; H, 4.06. Found: C, 36.38; H, 4.16. The higher C, H content is probably caused by minor amounts of $MoCl_3(PMe_2Ph)_3$, which also forms in this reaction (see Results section). The identity of the product as the face-sharing $Mo_2Cl_6(PMe_2Ph)_3$ is confirmed by X-ray crystallography and variable temperature NMR (see Results section). The product is slightly soluble in toluene and $CHCl_3$ and soluble in CH_2Cl_2 to generate dark purple solutions. UV/vis [CH_2Cl_2, λ/nm (ϵ/mol^{-1}·L·cm^{-1})]: 272 (sh) (20 500), 310 (17 600), 389 (sh) (1800), 515 (sh) (540), 590 (800). Crystals for the X-ray analysis have been obtained from hot toluene and by diffusion of *n*-heptane into a CH_2Cl_2 solution at room temperature.

Reaction of $Mo_2Cl_6(PMe_2Ph)_3$ with PMe_2Ph. Preparation of $Mo_2Cl_6(PMe_2Ph)_4$. $Mo_2Cl_6(PMe_2Ph)_3$ (117 mg, 0.143 mmol) was treated with PMe_2Ph (30 μL, 0.21 mmol) in 2 mL of $CHCl_3$. After a brief stirring, the red-brown solution was filtered, layered with 4 mL of *n*-heptane, and cooled to −20 °C. Brown crystals of the product $Mo_2Cl_6(PMe_2Ph)_4 \cdot 2CHCl_3$ formed over 48 h (yield 38 mg, 28%). One of these crystals was used for the X-ray analysis. UV/vis [CH_2Cl_2, room temperature, nm (ϵ/L·mol^{-1}·cm^{-1})]: 314 (22 000), 400 sh (2400), 526 (1100), 665 (640). χ_g: -0.0196×10^{-6} cgsu; diamagnetic correction (from Pascal's constants) $\chi_M = 614.5 \times 10^{-6}$ cgsu; $\chi_M^{cor} = 591 \times 10^{-6}$ cgsu; $\mu = 1.19\ \mu_B$ (0.84 μ_B/Mo atom).

Disproportionation of $Mo_2Cl_6(PEt_3)_4$. Preparation of $Mo_2Cl_6(PEt_3)_3 \cdot CH_2Cl_2$. $Mo_2Cl_6(PEt_3)_4$ (0.367 g, 0.418 mmol) was treated with 2 mL of CH_2Cl_2 to produce a brown solution that changed color over time at room temperature. The final solution had a dichroic behavior: deep forest green with fluorescent reflected light and reddish brown with refracted light. It was layered with 8 mL of *n*-heptane at room temperature. Dark purple crystals contaminated by a smaller amount of white crystals were obtained. A batch of the darker crystals was selected by handpicking. Their elemental analysis was slightly off that calculated for $Mo_2Cl_6(PEt_3)_3$ probably because of contamination by the white product and by variable amounts of CH_2Cl_2 of solvation. A single-crystal X-ray analysis (vide infra) and the NMR data (Results section) confirm the identity of this product as $Mo_2Cl_6(PEt_3)_3 \cdot CH_2Cl_2$. The white crystalline material was identified as a triethylphosphonium salt of a non-H-containing anion, presumably $[PHEt_3]^+Cl^-$. IR (Nujol mull/cm^{-1}): 2400 (P–H). ^1H NMR ($CDCl_3/\delta$): 1.40 (m, 3 H, CH_3), 2.31 (m, 2 H, CH_2). $^{31}P\{^1H\}$ NMR ($CDCl_3/\delta$): 19.95 (lit. 19.7 in CH_2Cl_2 for the bromide salt).[19]

An identical reaction was carried out in $CDCl_3$ and monitored by ^1H NMR spectroscopy. The formation of $Mo_2Cl_6(PEt_3)_3$ and $MoCl_3(PEt_3)_3$ was indicated; see the Results section.

Disproportionation of $Mo_2Cl_6(PEt_3)_4$ in THF. $Mo_2Cl_6(PEt_3)_4$ (ca. 100 mg) was dissolved in THF (5 mL). The resulting solution was stirred at room temperature. The color of the solution changed in a fashion similar to the corresponding run in CH_2Cl_2. Small aliquots of this solution (ca. 1 mL) were withdrawn periodically and evaporated to dryness and the residue dissolved in $CDCl_3$ for an NMR investigation. The NMR spectra were taken immediately after dissolution in $CDCl_3$ to avoid significant disproportionation in this solvent. The spectrum obtained after 15 days of stirring in THF was identical with that obtained after 24 h and corresponds to a mixture containing ca. 50% $Mo_2Cl_6(PEt_3)_4$, 33% $Mo_2Cl_6(PEt_3)_3$, and 17% $MoCl_3(PEt_3)_3$ (normalized to Mo atoms).

Thermal Treatment of $Mo_2Cl_6(PEt_3)_4$. Solid $Mo_2Cl_6(PEt_3)_4$ (0.301 g) was placed in a Schlenk tube, which was attached to a liquid-nitrogen-cooled trap and heated under vacuum overnight at ca. 145 °C. A total of 25.3 mg of PEt_3 was collected in the trap (62%). The waxy residue was dissolved in CH_2Cl_2 (4 mL), and the resulting solution was layered with 10 mL of *n*-heptane and cooled to −20 °C to produce a mixture of dark oil and crystals. The latter were separated from the mother solution and dried under vacuum. The ^1H NMR spectrum of a CD_2Cl_2 solution showed the presence of $Mo_2Cl_6(PEt_3)_3$ as the major product. The mother solution of this material was evaporated to dryness and the residue crystallized once more, this time from CH_2Cl_2 (4 mL) and Et_2O (15 mL) at −20 °C. A mixture of well-formed bright red and dark purple crystals was obtained. The dark purple product is $Mo_2Cl_6(PEt_3)_3$ (by ^1H NMR and UV/vis spectroscopy) while the red material is the known[20] $Mo_2Cl_4(PEt_3)_4$ as indicated by its ^{31}P NMR[20a] and UV/vis[20b] properties.

X-ray Crystallography. $Mo_2Cl_6(PMe_2Ph)_3$. A single crystal obtained from the recrystallization procedure in hot toluene was glued to the inside of a glass capillary, which was then sealed under a dinitrogen atmosphere and mounted on the diffractometer. The preliminary cell determination, the collection and reduction of intensity data, and the application of a correction for absorption[21a] were conducted in a routinely manner. Relevant crystal data are assembled in Table I. The molybdenum atoms were located by direct methods, and the rest of the structure was obtained by alternate cycles of full-matrix least-squares refinement and difference Fourier maps. The TEXSAN package of programs was used for the calculations. The hydrogen atoms were introduced at ideal positions and used for the calculation of the structure factors, but not refined. The structure converged to a final agreement factor $R = 0.038$. Selected bond distances and angles are listed in Table II.

The material crystallized from CH_2Cl_2/*n*-heptane was a mixture of plates and pyramidal-shaped crystals. The platelike crystals exhibited a unit cell that was, within experimental error, identical with that of the material crystallized from toluene. The pyramidal-shaped crystals exhibited a different unit cell (orthorhombic *C*-centered, $a = 20.047$ (4) Å, $b = 11.367$ (3) Å; $c = 15.160$ (4) Å, $V = 3454$ (1) Å^3 from the

(12) (a) Chakravarty, A. R.; Cotton, F. A.; Diebold, M. P.; Lewis, D. B.; Roth, W. J. *J. Am. Chem. Soc.* **1986**, *108*, 971. (b) Agaskar, P. A.; Cotton, F. A.; Dunbar, K. R.; Falvello, L. R.; O'Connor, C. J. *Inorg. Chem.* **1987**, *26*, 4051. (c) Owens, B. E.; Poli, R. *Polyhedron* **1989**, *8*, 545. (d) Cotton, F. A.; Fanwick, P. E.; Fitch, J. W. *Inorg. Chem.* **1978**, *17*, 3254. (e) Cotton, F. A.; Diebold, M. P.; O'Connor, C. J.; Powell, G. L. *J. Am. Chem. Soc.* **1985**, *107*, 7438. (f) Cotton, F. A. *Polyhedron* **1987**, *6*, 667.
(13) Wayda, A. L.; Darensbourg, M. Y.; Eds. *Experimental Organometallic Chemistry*; ACS Symposium Series 357; American Chemical Society: Washington, DC, 1987; Vol. 357.
(14) Anker, M. W.; Chatt, J.; Leigh, G. J.; Wedd, A. G. *J. Chem. Soc., Dalton Trans.* **1975**, 2639.
(15) Owens, B. E.; Poli, R.; Rheingold, A. L. *Inorg. Chem.* **1989**, *28*, 1456.
(16) Cotton, F. A.; Poli, R. *Inorg. Chem.* **1987**, *26*, 1514.
(17) Atwood, J. L.; Hunter, W. E.; Carmona-Guzman, E.; Wilkinson, G. *J. Chem. Soc., Dalton Trans.* **1980**, 4657.
(18) Reactions of phosphines with chlorinated hydrocarbons, usually leading to phosphorus quaternization, have been described: (a) Speziale, A. J.; Ratts, K. W. *J. Am. Chem. Soc.* **1962**, *84*, 854. (b) Appel, R. *Inorg. Synth.* **1986**, *24*, 107.
(19) Grim, S. O.; McFarlane, W. *Can. J. Chem.* **1968**, *46*, 2071.
(20) (a) San Filippo, J., Jr. *Inorg. Chem.* **1972**, *11*, 3140. (b) Cotton, F. A.; Daniels, L. M.; Powell, G. L.; Kahaian, A. J.; Smith, T. J.; Fiore Vogel, E. *Inorg. Chim. Acta* **1988**, *144*, 109.
(21) (a) North, A. C. T.; Phillips, D. C.; Mathews, F. S. *Acta Crystallogr., Sect. A* **1968**, *A24*, 351. (b) Walker, N.; Stuart, D. *Acta Crystallogr., Sect. A* **1983**, *A39*, 158.

Table I. Crystal Data for All Compounds

	$Mo_2Cl_6(PMe_2Ph)_3$	$Mo_2Cl_6(PEt_3)_3 \cdot CH_2Cl_2$	$Mo_2Cl_6(PMe_2Ph)_4 \cdot 2CHCl_3$
formula	$C_{24}H_{33}Cl_6Mo_2P_3$	$C_{19}H_{47}Cl_8Mo_2P_3$	$C_{34}H_{46}Cl_{12}Mo_2P_4$
fw	819.04	844.01	1195.95
space group	$P\bar{1}$	$P2_1/n$	$P\bar{1}$
a, Å	9.769 (1)	14.212 (2)	10.608 (3)
b, Å	12.9813 (6)	13.146 (3)	13.290 (3)
c, Å	13.744 (2)	19.090 (4)	18.810 (4)
α, deg	82.16 (1)	90	73.95 (2)
β, deg	76.299 (6)	99.61 (1)	86.17 (1)
γ, deg	82.16 (1)	90	77.11 (2)
V, Å^3	1603.9 (5)	3516 (2)	2484 (2)
Z	2	4	2
d_{calc}, g/cm^3	1.70	1.59	1.60
μ, cm^{-1}	128.07 (Cu Kα)	130.51 (Cu Kα)	12.88 (Mo Kα)
radiation (monochromated in incident beam)	Cu Kα (λ = 1.541 78 Å)	Cu Kα (λ = 1.541 78 Å)	Mo Kα (λ = 0.710 73 Å)
temp, °C	23	23	22
transm factors: max, min	1.000, 0.393	1.000, 0.208	1.000, 0.886
R^a	0.038	0.080	0.034
$R_w{}^b$	0.061	0.099	0.047

$^a R = \sum||F_o| - |F_c||/\sum|F_o|$. $^b R_w = [\sum w(|F_o| - |F_c|)^2/\sum w|F_o|^2]^{1/2}$; $w = 1/\sigma^2(|F_o|)$.

least-squares refinement of the setting angles of 11 reflections in the 30° < 2θ < 40° range, Cu Kα radiation). It was hoped that this form might consist of the gauche isomer (see Results section) of the $Mo_2Cl_6(PMe_2Ph)_3$ compound. The unit cell volume fits four molecules of $Mo_2Cl_6(PMe_2Ph)_3$, which, because of the lattice symmetry and the double cell, must be located on a 2-fold symmetry operator in a noncentrosymmetric space group. Therefore, this compound could not be the sought gauche isomer, which cannot contain any molecular symmetry operator. On the grounds that this is probably a different crystalline form of the same isomer (no evidence of other species was obtained from the NMR analysis, see Results section), it was deemed unnecessary to collect a data set on this form.

$Mo_2Cl_6(PEt_3)_3 \cdot CH_2Cl_2$. A single crystal was glued to the inside of a glass capillary, which was then sealed under a dinitrogen atmosphere and mounted on the diffractometer. The preliminary cell determination, the collection and reduction of intensity data, and the application of a correction for absorption[21a] were conducted in a routine manner. Relevant crystal data are assembled in Table I. Direct methods revealed the position of the two molybdenum atoms and most of the coordination sphere. The remainder of the structure was located by alternate full-matrix least-squares cycles of refinement and difference Fourier maps by using the TEXSAN package of programs. Hydrogen atoms were introduced at calculated positions and used for the structure factors calculations, but not refined. An additional absorption correction[21b] was applied before anisotropic refinement of the non-hydrogen atoms. Selected bond distances and angles are compared with those of the corresponding PMe_2Ph structure in Table II.

$Mo_2Cl_6(PMe_2Ph)_4 \cdot 2CHCl_3$. A single crystal was glued to the inside of a glass capillary, which was then sealed under a dinitrogen atmosphere and mounted on the diffractometer. Preliminary operations and data collection and reduction were carried out as described for the above two compounds, including the application of an absorption correction.[21a] In addition, a decay correction was applied. Three periodicaly monitored intensity standards revealed an average decay of 13% over the data collection. Relevant crystal data are given in Table I. The position of the molybdenum atoms was obtained from a Patterson analysis, and the structure was expanded with the program DIRDIF. All the non-hydrogen atoms of the $Mo_2Cl_6(PMe_2Ph)_4$ molecule were located in this manner. Subsequent isotropic full-matrix least-squares refinement converged to R = 0.18 and a difference Fourier map revealed the position of two ordered chloroform interstitial molecules. The inclusion of these led to isotropic convergence at R = 0.079. Refinement was continued by treating all atoms anisotropically and by finally including the hydrogen atoms in calculated positions with an isotropic thermal parameter equal to 1.2 times the equivalent isotropic parameter of the attached carbon atoms and using these atoms only for structure factor calculation. All calculations were carried out with the TEXSAN package of programs. Selected bond distances and angles are listed in Table III.

Fenske–Hall Molecular Orbital Calculations.[22] Calculations were carried out on the model compounds $Mo_2Cl_6(PH_3)_3$ and $Mo_2Cl_6(PH_3)_4$ at various metal–metal bond distances. Atomic parameters were obtained from the crystal structures of $Mo_2Cl_6(PEt_3)_3 \cdot CH_2Cl_2$ and $Mo_2Cl_6(PMe_2Ph)_4 \cdot 2CHCl_3$ by averaging all chemically equivalent parameters and idealizing to C_s symmetry the former and to C_2 the latter (the C_2 axis passing through the metal–metal vector). The hydrogen atoms were placed at 1.44 Å from the phosphorus atoms, keeping the bond angles as found in the crystal structures but idealizing the conformation of the PH_3 group in order to achieve the maximum symmetry. The parameters for structures with different metal–metal separations were obtained by keeping the bond distances to the bridging chlorine atoms constant and accordingly varying the angles at the central moiety [$Mo_2(\mu\text{-}Cl)_3$ for face-sharing molecules and $Mo_2(\mu\text{-}Cl)_2$ for edge-sharing molecules]. The remaining terminal ligands were allowed to "ride" on the metal atoms, thereby keeping all parameters for the terminal groups constant. A minimum basis set was employed. The atomic 1s, 2s, 2p, 3s, 3p, 3d, 4s, and 4p orbitals of the Mo atoms and the 1s, 2s, and 2p orbitals of the Cl and P atoms were treated as "core". The basis functions used were STO's with coefficients and exponents obtained from Prof. M. B. Hall. A right-handed coordinate system was chosen, with the Mo–Mo vector along the z axis and the origin equidistant from the two metals for each molecule. The face-sharing bioctahedral molecules were placed with one of the three bridging chlorine atoms lying on the x axis. The edge-sharing bioctahedral molecules were placed with the plane determined by the central Mo_2Cl_2 moiety perpendicular to the x axis. The local coordinate system in each molecule was such that the two metal atoms pointed their z axis toward each other, the bridging chlorine atoms pointed their z axis toward the origin, and all the terminal chlorine and phosphorus atoms pointed their z axis at the corresponding molybdenum atom.

Results

(a) Syntheses and Reactivity Studies. The interaction of $MoX_3(THF)_3$ (X = Cl, Br, I) with 3 equiv of tertiary phosphine proceeds smoothly in THF as already described[14-17] (see eq 1).

$$MoX_3(THF)_3 + 3L \xrightarrow{THF} MoX_3L_3 + 3THF \qquad (1)$$

The reaction is faster for the heavier halide derivative: for X = I, ca. 10 min; for X = Br, ca. 1.5 h; and for X = Cl, overnight stirring at room temperature were required to attain a complete transformation.

The face-sharing bioctahedral $Mo_2Cl_6(PMe_2Ph)_3$ derivative was prepared by a procedure similar to that used[11] to obtain the edge-sharing bioctahedral $Mo_2Cl_6(PEt_3)_4$ adduct (indeed, the PMe_2Ph analogue of the latter compound was our original target). Interaction between $MoCl_3(THF)_3$ and 2 equiv of the phosphine in THF, followed by brief thermal treatment in toluene, afforded a mixture of a very dark crystalline material and a yellow solution. The solid is the confacial bioctahedral $Mo_2Cl_6(PMe_2Ph)_3$, as shown by elemental analysis, ^{1}H NMR spectroscopy, and X-ray crystallography (vide infra), while the mother solution contains the mononuclear tris adduct (eq 2). The confacial bioctahedral molecule has been subsequently obtained in higher yields by using the P:Mo stoichiometric ratio of 3:2 under conditions similar to those outlined in eq 2.

$$3MoCl_3(THF)_3 + 6PMe_2Ph \xrightarrow{(1)\ THF} \xrightarrow{(2)\ toluene/\Delta} Mo_2Cl_6(PMe_2Ph)_3 + MoCl_3(PMe_2Ph)_3 \qquad (2)$$

(22) Hall, M. B.; Fenske, R. F. *Inorg. Chem.* **1972**, *11*, 768.

Table II. Selected Bond Distances (Å) and Angles (deg) for $Mo_2Cl_6(PMe_2Ph)_3$ and $Mo_2Cl_6(PEt_3)_3 \cdot CH_2Cl_2$

(a) Distances

	PMe_2Ph		PEt_3	
Mo–Mo	Mo(1)–Mo(2)	2.6582 (5)	Mo(1)–Mo(2)	2.753 (2)
Mo–(μ-Cl)	Mo(1)–Cl(1)	2.520 (1)	Mo(1)–Cl(4)	2.504 (3)
	Mo(1)–Cl(2)	2.483 (1)	Mo(1)–Cl(3)	2.459 (4)
	Mo(1)–Cl(3)	2.465 (1)	Mo(1)–Cl(5)	2.463 (4)
	Mo(2)–Cl(1)	2.444 (1)	Mo(2)–Cl(4)	2.431 (4)
	Mo(2)–Cl(2)	2.479 (1)	Mo(2)–Cl(3)	2.477 (3)
	Mo(2)–Cl(3)	2.485 (1)	Mo(2)–Cl(5)	2.487 (4)
Mo–Cl	Mo(1)–Cl(4)	2.366 (1)	Mo(1)–Cl(2)	2.367 (4)
	Mo(1)–Cl(5)	2.373 (1)	Mo(1)–Cl(1)	2.380 (4)
	Mo(2)–Cl(6)	2.374 (1)	Mo(2)–Cl(6)	2.382 (4)
Mo–P	Mo(1)–P(1)	2.530 (1)	Mo(1)–P(1)	2.541 (4)
	Mo(2)–P(2)	2.552 (1)	Mo(2)–P(2)	2.575 (4)
	Mo(2)–P(3)	2.575 (1)	Mo(2)–P(3)	2.555 (4)

(b) Angles

	PMe_2Ph		PEt_3	
(μ-Cl)–Mo–(μ-Cl)	Cl(1)–Mo(1)–Cl(2)	95.99 (4)	Cl(3)–Mo(1)–Cl(4)	94.2 (1)
	Cl(1)–Mo(1)–Cl(3)	91.68 (4)	Cl(4)–Mo(1)–Cl(5)	92.4 (1)
	Cl(2)–Mo(1)–Cl(3)	92.55 (4)	Cl(3)–Mo(1)–Cl(5)	88.3 (1)
	Cl(1)–Mo(2)–Cl(2)	98.08 (4)	Cl(3)–Mo(2)–Cl(4)	95.6 (1)
	Cl(1)–Mo(2)–Cl(3)	93.06 (4)	Cl(4)–Mo(2)–Cl(5)	93.6 (1)
	Cl(2)–Mo(2)–Cl(3)	92.17 (4)	Cl(3)–Mo(2)–Cl(5)	87.4 (1)
(μ-Cl)–Mo–L	Cl(1)–Mo(1)–Cl(4)	88.06 (5)	Cl(2)–Mo(1)–Cl(4)	89.1 (1)
	Cl(1)–Mo(1)–Cl(5)	90.84 (5)	Cl(1)–Mo(1)–Cl(4)	87.9 (1)
	Cl(1)–Mo(1)–P(1)	177.81 (5)	Cl(4)–Mo(1)–P(1)	178.2 (2)
	Cl(2)–Mo(1)–Cl(4)	175.84 (5)	Cl(2)–Mo(1)–Cl(3)	176.6 (1)
	Cl(2)–Mo(1)–Cl(5)	87.35 (5)	Cl(1)–Mo(1)–Cl(3)	89.9 (1)
	Cl(2)–Mo(1)–P(1)	82.06 (4)	Cl(3)–Mo(1)–P(1)	87.3 (1)
	Cl(3)–Mo(1)–Cl(4)	88.24 (5)	Cl(2)–Mo(1)–Cl(5)	90.9 (1)
	Cl(3)–Mo(1)–Cl(5)	177.48 (5)	Cl(1)–Mo(1)–Cl(5)	178.2 (2)
	Cl(3)–Mo(1)–P(1)	87.41 (4)	Cl(5)–Mo(1)–P(1)	86.7 (1)
	Cl(1)–Mo(2)–Cl(6)	172.24 (5)	Cl(4)–Mo(2)–Cl(6)	172.3 (1)
	Cl(1)–Mo(2)–P(2)	88.87 (4)	Cl(4)–Mo(2)–P(2)	88.8 (1)
	Cl(1)–Mo(2)–P(3)	81.64 (4)	Cl(4)–Mo(2)–P(3)	85.1 (1)
	Cl(2)–Mo(2)–Cl(6)	87.72 (5)	Cl(3)–Mo(2)–Cl(6)	90.3 (1)
	Cl(2)–Mo(2)–P(2)	171.61 (5)	Cl(3)–Mo(2)–P(2)	172.4 (1)
	Cl(2)–Mo(2)–P(3)	86.22 (4)	Cl(3)–Mo(2)–P(3)	86.4 (1)
	Cl(3)–Mo(2)–Cl(6)	91.86 (5)	Cl(5)–Mo(2)–Cl(6)	91.8 (1)
	Cl(3)–Mo(2)–P(2)	82.73 (4)	Cl(5)–Mo(2)–P(2)	86.1 (1)
	Cl(3)–Mo(2)–P(3)	174.17 (4)	Cl(5)–Mo(2)–P(3)	173.5 (1)
L–Mo–L	Cl(4)–Mo(1)–Cl(5)	91.69 (5)	Cl(1)–Mo(1)–Cl(2)	90.8 (2)
	Cl(4)–Mo(1)–P(1)	93.90 (5)	Cl(2)–Mo(1)–P(1)	89.3 (1)
	Cl(5)–Mo(1)–P(1)	90.08 (5)	Cl(1)–Mo(1)–P(1)	93.0 (1)
	Cl(6)–Mo(2)–P(2)	85.80 (5)	Cl(6)–Mo(2)–P(2)	86.0 (1)
	Cl(6)–Mo(2)–P(3)	93.67 (5)	Cl(6)–Mo(2)–P(3)	90.2 (1)
	P(2)–Mo(2)–P(3)	99.50 (4)	P(2)–Mo(2)–P(3)	100.2 (1)
Mo–(μ-Cl)–Mo	Mo(1)–Cl(1)–Mo(2)	64.74 (3)	Mo(1)–Cl(4)–Mo(2)	67.8 (1)
	Mo(1)–Cl(2)–Mo(2)	64.78 (3)	Mo(1)–Cl(3)–Mo(2)	67.80 (9)
	Mo(1)–Cl(3)–Mo(2)	64.97 (3)	Mo(1)–Cl(5)–Mo(2)	67.6 (1)

The edge-sharing PMe_2Ph dimer has been obtained by interacting the face-sharing dimer with phosphine in $CHCl_3$. ^1H NMR monitoring established that this interaction proceeds as illustrated in eqs 3 and 4. Equation 3 is rapid (complete within a few minutes

$$Mo_2Cl_6(PMe_2Ph)_3 + PMe_2Ph \xrightarrow{fast} Mo_2Cl_6(PMe_2Ph)_4 \quad (3)$$

$$Mo_2Cl_6(PMe_2Ph)_4 + 2PMe_2Ph \xrightarrow{slow} 2MoCl_3(PMe_2Ph)_3 \quad (4)$$

at room temperature), whereas eq 4 takes a much longer time. Thus, the use of a small excess of PMe_2Ph over the 1:1 phosphine:dimer ratio and short exposure to room temperature maximize the yields of the edge-sharing dimer.

The edge-sharing bioctahedral $Mo_2Cl_6(PMe_2Ph)_4$ slowly and quantitatively (by ^1H NMR) disproportionates at room temperature in $CDCl_3$ as shown in eq 5. A small amount of free

$$3Mo_2Cl_6(PMe_2Ph)_4 \rightarrow 2Mo_2Cl_6(PMe_2Ph)_3 + 2MoCl_3(PMe_2Ph)_3 \quad (5)$$

PMe_2Ph is observed at the end of the disproportionation reaction (^{31}P NMR peak at δ −44.3). This reaction has also been monitored by UV/visible spectroscopy in CH_2Cl_2. Isosbestic points were observed at 399, 581, and 632 nm.

A disproportionation analogous to that shown in eq 5 also occurs for the previously reported $Mo_2Cl_6(PEt_3)_4$ complex,[11] with formation of the face-sharing bioctahedral $Mo_2Cl_6(PEt_3)_3$ and the mononuclear $MoCl_3(PEt_3)_3$ compounds (eq 6). This transfor-

$$3Mo_2Cl_6(PEt_3)_4 \rightarrow 2Mo_2Cl_6(PEt_3)_3 + 2MoCl_3(PEt_3)_3 \quad (6)$$

mation also appears quantitative when carried out in $CDCl_3$. Free PEt_3 is also formed, as evidenced by ^{31}P NMR (resonance at −17.4 δ). UV/visible monitoring of this reaction shows isosbestic points at 371, 454, and 505 nm when $CHCl_3$ was used as solvent, but the same behavior is not observed in CH_2Cl_2. This difference can be ascribed to the reaction of free phosphine with the CH_2Cl_2 solvent[18] and provides additional evidence for the generation of free phosphine during the disproportionation reaction. We have isolated the $Mo_2Cl_6(PEt_3)_3$ product from this reaction carried out

Table III. Selected Intramolecular Distances (Å) and Angles (deg) and Estimated Standard Deviations for $Mo_2Cl_6(PMe_2Ph)_4 \cdot 2CHCl_3$

Distances			
Mo(1)–Mo(2)	2.8036 (8)	Mo(2)–Cl(1)	2.420 (1)
Mo(1)–Cl(1)	2.380 (1)	Mo(2)–Cl(2)	2.416 (1)
Mo(1)–Cl(2)	2.386 (1)	Mo(2)–Cl(3)	2.401 (1)
Mo(1)–Cl(5)	2.438 (1)	Mo(2)–Cl(4)	2.395 (1)
Mo(1)–Cl(6)	2.444 (2)	Mo(2)–P(3)	2.569 (1)
Mo(1)–P(1)	2.571 (1)	Mo(2)–P(4)	2.597 (2)
Mo(1)–P(2)	2.582 (1)		
Angles			
Mo(2)–Mo(1)–Cl(1)	54.93 (3)	Mo(1)–Mo(2)–Cl(2)	53.77 (3)
Mo(2)–Mo(1)–Cl(2)	54.79 (4)	Mo(1)–Mo(2)–Cl(3)	100.01 (4)
Mo(2)–Mo(1)–Cl(5)	136.93 (4)	Mo(1)–Mo(2)–Cl(4)	98.25 (4)
Mo(2)–Mo(1)–Cl(6)	136.65 (4)	Mo(1)–Mo(2)–P(3)	129.70 (3)
Mo(2)–Mo(1)–P(1)	98.25 (4)	Mo(1)–Mo(2)–P(4)	133.46 (4)
Mo(2)–Mo(1)–P(2)	97.85 (4)	Cl(1)–Mo(2)–Cl(2)	107.36 (5)
Cl(1)–Mo(1)–Cl(2)	109.69 (5)	Cl(1)–Mo(2)–Cl(3)	90.91 (4)
Cl(1)–Mo(1)–Cl(5)	82.08 (5)	Cl(1)–Mo(2)–Cl(4)	101.01 (4)
Cl(1)–Mo(1)–Cl(6)	167.83 (4)	Cl(1)–Mo(2)–P(3)	76.75 (4)
Cl(1)–Mo(1)–P(1)	95.00 (4)	Cl(1)–Mo(2)–P(4)	168.28 (4)
Cl(1)–Mo(1)–P(2)	92.22 (5)	Cl(2)–Mo(2)–Cl(3)	99.45 (5)
Cl(2)–Mo(1)–Cl(5)	167.50 (5)	Cl(2)–Mo(2)–Cl(4)	90.28 (5)
Cl(2)–Mo(1)–Cl(6)	82.10 (5)	Cl(2)–Mo(2)–P(3)	172.15 (4)
Cl(2)–Mo(1)–P(1)	92.95 (4)	Cl(2)–Mo(2)–P(4)	80.24 (5)
Cl(2)–Mo(1)–P(2)	98.34 (4)	Cl(3)–Mo(2)–Cl(4)	161.69 (5)
Cl(5)–Mo(1)–Cl(6)	86.42 (5)	Cl(3)–Mo(2)–P(3)	87.04 (5)
Cl(5)–Mo(1)–P(1)	81.55 (4)	Cl(3)–Mo(2)–P(4)	78.87 (5)
Cl(5)–Mo(1)–P(2)	85.02 (4)	Cl(4)–Mo(2)–P(3)	82.30 (5)
Cl(6)–Mo(1)–P(1)	87.17 (5)	Cl(4)–Mo(2)–P(4)	87.64 (5)
Cl(6)–Mo(1)–P(2)	82.83 (5)	P(3)–Mo(2)–P(4)	96.83 (5)
P(1)–Mo(1)–P(2)	163.71 (5)	Mo(1)–Cl(1)–Mo(2)	71.47 (4)
Mo(1)–Mo(2)–Cl(1)	53.61 (4)	Mo(1)–Cl(2)–Mo(2)	71.44 (4)

in preparative scale. The same disproportionation occurs in THF. However, an equilibrium mixture of face-sharing dimer, monomer, and unreacted edge-sharing dimer was obtained in this solvent corresponding to ca. 50% convertion. No THF-containing complexes were observed by NMR.

The $Mo_2Cl_6(PEt_3)_3$ material has also been obtained by warming the solid $Mo_2Cl_6(PEt_3)_4$ at 145 °C under vacuum in a manner similar to the reported formation of $W_2Cl_6(PEt_3)_3$ from $W_2Cl_6(PEt_3)_4$.[23] The molybdenum system, however, appears to be more sensitive to high temperatures with respect to the tungsten system since small amounts of the known[20] $Mo_2Cl_4(PEt_3)_4$ compound were also produced along an unknown decomposition pathway.

Interaction of $Mo_2Cl_6(PEt_3)_3$ and PEt_3 follows the same pathway described above for the analogous PMe_2Ph system (eqs 7 and 8). Reaction 7 is less rapid then reaction 3, but it is still much faster than the subsequent monomer formation (reaction 8), so that the edge-sharing dimer accumulates in solution in significant amounts.

$$Mo_2Cl_6(PEt_3)_3 + PEt_3 \xrightarrow{\text{fast}} Mo_2Cl_6(PEt_3)_4 \quad (7)$$

$$Mo_2Cl_6(PEt_3)_4 + 2PEt_3 \xrightarrow{\text{slow}} 2MoCl_3(PEt_3)_3 \quad (8)$$

(b) NMR Studies. Nuclear magnetic resonance studies of paramagnetic, octahedrally coordinated d^3 systems were limited to vanadium(II), chromium(III), and one compound of tungsten(III), i.e. $WCl_3(PMe_3)_3$.[10c] We have recently reported the ^1H NMR properties of the tetrahydrofuran adducts $MoX_3(THF)_3$ (X = Cl, Br).[24] We have now investigated molybdenum systems of types I, II, and III, where L = phosphine, by ^1H NMR.

Mononuclear Compounds. This paper is mainly concerned with mononuclear and dinuclear Mo(III) compounds with the phosphine ligands PEt_3 and PMe_2Ph. However, we have also investigated the ^1H NMR properties of the prototypic mononuclear PMe_3 complexes, $MoX_3(PMe_3)_3$ (X = Cl, Br, I). Both meridional and facial structures are possible in principle for these compounds. For similar compounds, the *mer* structure has been typically found in the solid state unless the three neutral ligands are part of the same polydentate unit which demands three mutually cis coordination positions.[15] Studies of the stereochemistry in solution, to the best of our knowledge, were not available prior to our ^1H NMR investigations.

The spectra of $MoX_3(PMe_3)_3$ (Figure 1) show two peaks in a 1:2 ratio, consistent with a meridional geometry. There is no other peak in the spectra. Therefore, if any facial isomer is present, its maximum level is estimated to be not higher than ca. 1%. These peaks are at higher fields with respect to the position of the free ligand and shift further upfield upon lowering the temperature. There is a linear dependence of the chemical shift with the inverse temperature (see Figure 1). This is in accord with the general theory of paramagnetic NMR since both the dipolar contribution and the Fermi contact contribution to the paramagnetic shift depend linearly on the magnetic susceptibility and thus also on the inverse temperature for a system that obeys the Curie law.[25] The paramagnetic shift of the unique phosphine protons (trans to X; relative intensity 1) is in the order I > Br > Cl, whereas the shift of the other protons (the two phosphines trans to each other, relative intensity 2) is in the opposite order. The lines are broadest (width at half-height ca. 300 Hz at room temperature) for X = Cl and sharpest (ca. 120 Hz) for X = I.

The $MoX_3(PMe_2Ph)_3$ (X = Cl, Br, I) derivatives have a similar behavior (Figure 1). The methyl proton resonances for these derivatives are in the same region as those of $MoX_3(PMe_3)_3$ and exhibit the expected 1:2 pattern for the meridional configuration. The phenyl protons, on the other hand, are shifted downfield. Each set of protons (ortho, meta, and para) is also separated into two resonances in a 1:2 relative ratio. In the absence of labeling studies, we tentatively assign the broader and more paramagnetically shifted peaks to the ortho protons, which are closer to the paramagnetic center. The signals of the para protons are easily identified because their intensity is half that of the ortho and meta protons, and they are in fact the least paramagnetically shifted as expected from their larger distance from the molybdenum center. The variable-temperature behavior of these spectra parallels the one described above for the PMe_3 compounds (see Figure 1).

The $MoCl_3(PEt_3)_3$ compound has not been isolated. However, its ^1H NMR spectrum has been obtained from the reactivity study of the corresponding dinuclear compounds (vide supra, reactions 6 and 8). The methylene protons resonate in the same region of the α-protons as the other monomers described above [$MoCl_3(PMe_3)_3$ and $MoCl_3(PMe_2Ph)_3$], that is at δ −24.8 and −31.1 (1:2 ratio) at 295 K. The methyl protons are shifted downfield, at δ 12.9 and 10.6 (1:2 ratio) at the same temperature.

Edge-Sharing Bioctahedral Compounds, $Mo_2Cl_6L_4$ (L = PEt_3, PMe_2Ph). As stated above, these compounds decompose by disproportionation to face-sharing dimer and monomer (eqs 5 and 6) upon dissolution in $CDCl_3$. However, the decomposition is slow below room temperature, and a variable-temperature ^1H NMR investigation could be carried out.

The ^1H NMR resonances of pure $Mo_2Cl_6(PEt_3)_4$ are given in Figure 2. The two downfield resonances are due to the methyl protons and the two upfield resonances correspond to the methylene protons (relative intensity 3:3:2:2). Thus, ^1H NMR spectroscopy shows that the four phosphine ligands are equally distributed among two distinct chemical environments, in perfect agreement with the previously reported crystal structure, which shows an edge-sharing bioctahedral arrangement with two axial and two equatorial phosphine ligands.[11] We conclude that the solid-state structure is maintained in solution.

The ^1H NMR paramagnetic shifts of $Mo_2Cl_6(PEt_3)_4$ are only slightly reduced with respect to the $S = {}^3/_2$ $MoCl_3(PEt_3)_3$ system, and the temperature dependence of the resonances shows Curie

(23) Chacon, S. T.; Chisholm, M. H.; Streib, W. E.; Van Der Sluys, W. *Inorg. Chem.* **1989**, *28*, 6.
(24) Poli, R.; Mui, H. D. *J. Am. Chem. Soc.* **1990**, *112*, 2446.
(25) Jesson, J. P. In *NMR of Paramagnetic Molecules: Principles and Applications*; La Mar, G. N., Horrocks, W. DeW., Jr., Holm, R. H., Eds., Academic Press: New York and London, 1973; Chapter 1.

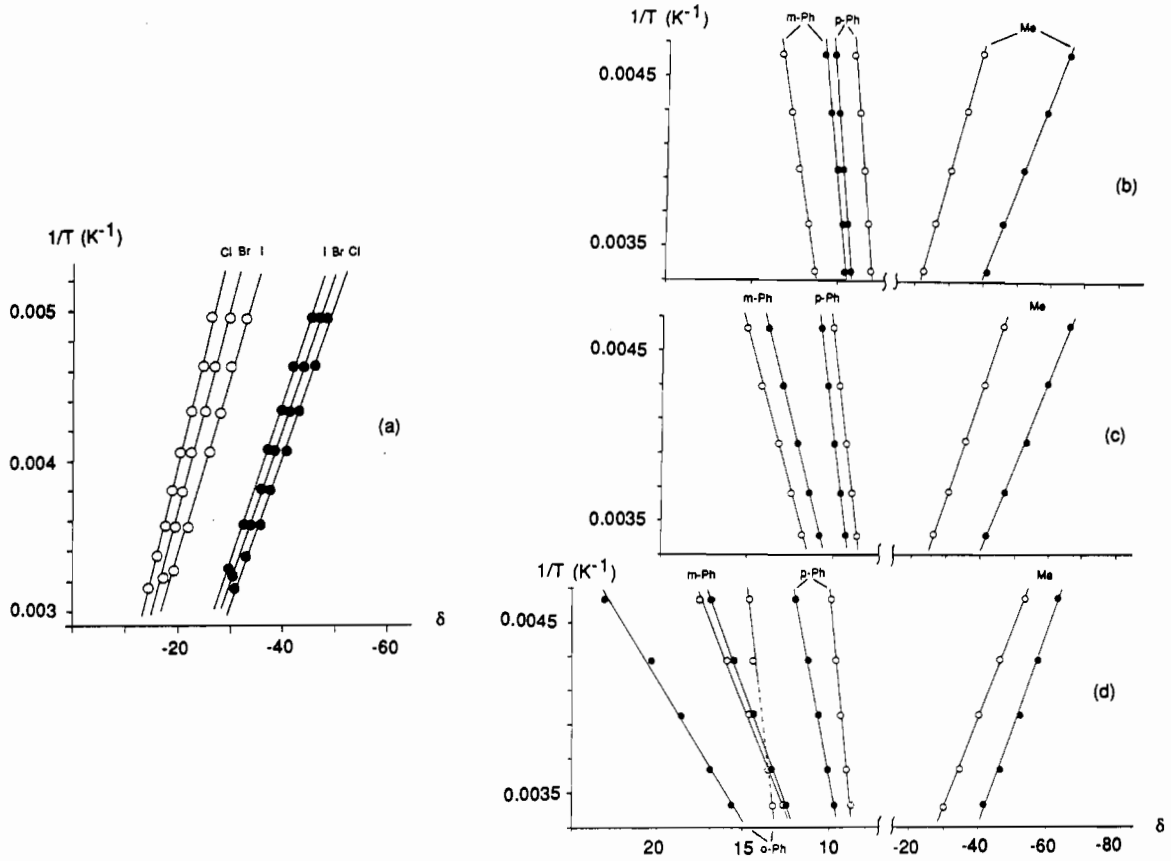

Figure 1. Variable-temperature ^1H NMR properties of *mer*-MoX_3L_3 (X = Cl, Br, I; solvent = $CDCl_3$): (a) L = PMe_3; (b) $MoCl_3(PMe_2Ph)_3$; (c) $MoBr_3(PMe_2Ph)_3$; (d) $MoI_3(PMe_2Ph)_3$. For each set of protons, white circles indicate the resonances of relative intensity 1 and black circles indicate the resonances of relative intensity 2. For the $MoX_3(PMe_2Ph)_3$ (X = Cl, Br) derivatives, the Ph ortho H resonances were too broad and overlapping with the meta H resonances for the positions of their maximums to be accurately measured.

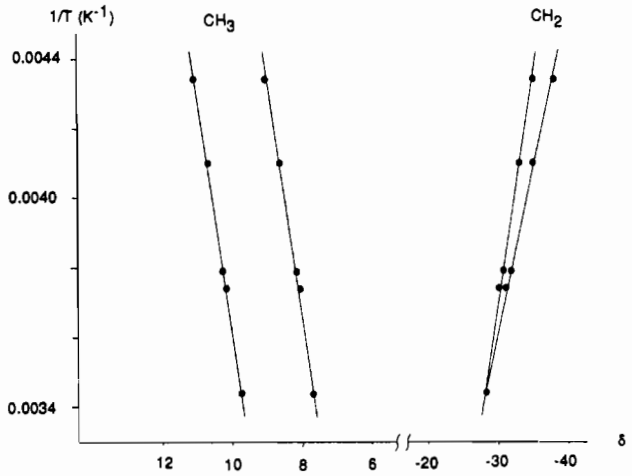

Figure 2. Variable-temperature ^1H NMR properties of $Mo_2Cl_6(PEt_3)_4$ (solvent = $CDCl_3$).

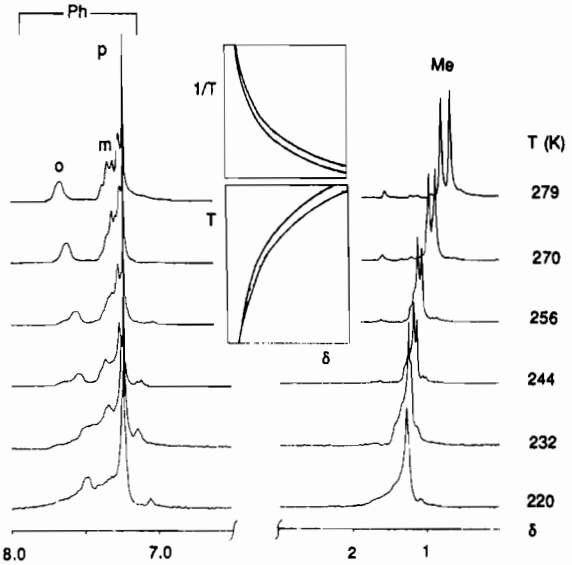

Figure 3. Variable-temperature ^1H NMR properties of $Mo_2Cl_6(PMe_2Ph)_4$ (solvent = $CDCl_3$). The insets show the dependence of δ on T (upper) and $1/T$ (lower) for the methyl proton resonances.

behavior in the range investigated. This is consistent with the previously reported room-temperature magnetic moment for the solid,[11] which is only slightly reduced with respect to the calculated value for noninteracting Mo(III) centers.

The ^1H NMR spectrum of $Mo_2Cl_6(PMe_2Ph)_4$ (Figure 3) is consistent for a structure identical with that of the PEt_3 counterpart. This is confirmed by a crystallographic study (vide infra). However, the paramagnetic contact shifts for all the signals are much reduced. The methyl protons appear as two singlets in a 1:1 ratio at room temperature. The phenyl protons appear as complex multiplets and cannot be used for structural assignments. The broadest and more shifted multiplet is assigned to the ortho protons, followed by meta and para as the paramagnetic shift decreases. The alternative possibility that the methyl protons are all equivalent and appear as a doublet because of coupling to the ^{31}P nucleus cannot be ruled out but appears unlikely because (i) no ^{31}P NMR signal is observed, presumably because of the vicinity of the phosphorus nuclei to the source of paramagnetism, which causes a very rapid relaxation of the ^{31}P nuclear spin states with consequent line broadening. In such a situation, coupling to the proton nuclei is not anticipated. (ii) The solid-state geometry of $Mo_2Cl_6(PMe_2Ph)_4$ is identical with the solid-state[11] and solution geometry of $Mo_2Cl_6(PEt_3)_4$. The methyl signals appear as a sharp 1:1 feature at room temperature. This shows that all the phosphine

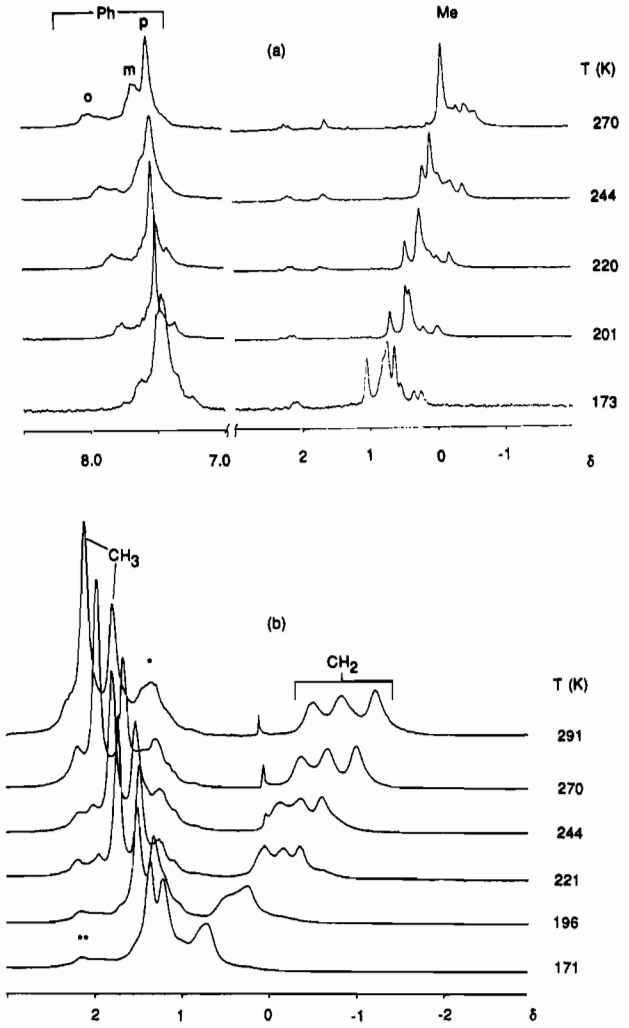

Figure 4. Variable-temperature ^1H NMR properties of the $Mo_2Cl_6L_3$ compounds (solvent = CD_2Cl_2): (a) L = PMe_2Ph; (b) L = PEt_3. Single and double asterisks denote temperature-independent peaks, probably due to the $[PHEt_3]^+Cl^-$ impurity.

ligands are freely rotating around the Mo–P axes under these conditions. However, the signals considerably broaden at lower temperature until they coalesce in a single broad peak, as a possible result of hindered rotation.

The paramagnetic shifts for $Mo_2Cl_6(PMe_2Ph)_4$, like those of its PEt_3 congener, are temperature dependent. However, contrary to the corresponding PEt_3 compound, the shifts *decrease* upon lowering the temperature (see Figure 3). This effect is in accord with a much stronger magnetic coupling between the two molybdenum centers and is probably the result of a stronger metal–metal bonding (see next section and the Discussion section). Solid-state magnetic susceptibility measurements show that the compound is practically diamagnetic (0.84 μ_B/Mo atom; we cannot exclude that part of this paramagnetism is due to mononuclear impurities), in accord with the NMR and crystallographic data.

Confacial Bioctahedral Compounds. The ^1H NMR spectra of compounds $Mo_2Cl_6L_3$ (L = PEt_3, PMe_2Ph) are also paramagnetically shifted with respect to the free ligand. The spectra and their variation with temperature are illustrated in Figure 4. Analogous to the mononuclear and edge-sharing bioctahedral derivatives discussed above, the face-sharing bioctahedral dimers show upfield shifts for the α-protons (CH_2 protons for the PEt_3 compound, Me protons for the PMe_2Ph compound) and downfield shifts for the other protons (Me protons for the PEt_3 compound and Ph protons for the PMe_2Ph compound). At the same temperature, the phosphine α-protons are slightly more shifted for the PEt_3 compound. Contrary to the mononuclear compounds and to $Mo_2Cl_6(PEt_3)_4$, but similar to $Mo_2Cl_6(PMe_2Ph)_4$, the paramagnetic shifts are small and decrease upon cooling.

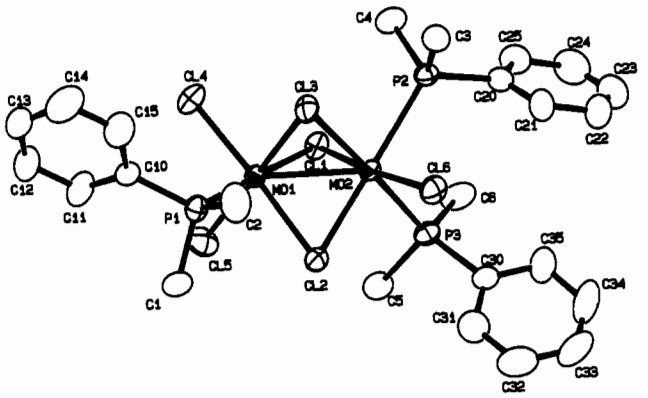

Figure 5. ORTEP view of the $Mo_2Cl_6(PMe_2Ph)_3$ structure with the numbering scheme employed. The ORTEP plot files were modified with the program PLOTMD for label position optimization.[50]

The number of peaks observed carry important structural information. As will be shown in the next section, the compounds crystallize in the anti configuration (Ia). If such a structure were

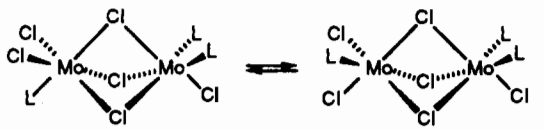

retained in solution, three peaks for the α-protons would be expected for the PEt_3 derivative (1:1:1 relative ratio) and three for the PMe_2Ph derivatives (1:1:1 ratio), assuming free rotation around the Mo–P bonds. The spectra in Figure 4 show that, at least for the PMe_2Ph compound, a more complex pattern is observed in the α-proton region, all signals having a similar dependence on temperature. These extra signals can be accounted for by the presence in solution of the gauche isomer in equilibrium with the anti isomer.

An equilibrium of this kind has been described before for $Mo_2Cl_6(SMe_2)_3$[26] and for the $[Mo_2X_7(PMe_3)_2]^-$ (X = Cl, I)[27] anions (generating, in that case, syn and gauche isomers). For $[Mo_2Cl_7(PMe_3)_2]^-$, both forms have been crystallographically characterized.[27b] These anions, analogous to the neutral confacial bioctahedral compounds, exhibit paramagnetic shifts for the methyl protons. An anti–gauche isomerism has also been proposed to occur for the $Mo_2X_6(THF)_3$ (X = Cl, Br) derivatives.[24]

(c) Crystallographic Studies. $Mo_2Cl_6L_3$ (L = PMe_2Ph, PEt_3). Neutral confacial bioctahedral $LX_2Mo(\mu\text{-}X)_3MoXL_2$ compounds of Mo(III) with monodentate ligands have been reported earlier[14,28,29] but their structures have not been demonstrated by crystallographic studies as of the beginning of the present investigation. The crystal structure of $Mo_2Cl_6(THT)_3$ (type Ia; THT = tetrahydrothiophene) has recently appeared[26b] together with ^1H NMR evidence for several different isomers. The crystal structure of a derivative with three chelating ligands, $Mo_2(\mu\text{-}SC_6H_4\text{-}o\text{-}PPh_2)_3Cl_3$, has also been reported recently,[30] and we have been informed of the structural characterization of $Mo_2Cl_6(PEt_3)_3$ in a different crystalline form with respect to that reported here.[31]

The $Mo_2Cl_6L_3$ (L = PMe_2Ph, PEt_3) compounds have been crystallographically characterized by single-crystal X-ray dif-

(26) (a) Boorman, P. M.; Moynihan, K. J.; Oakley, R. T. *J. Chem. Soc., Chem. Commun.* **1982**, 899. (b) Moynihan, K. J.; Gao, X.; Boorman, P. M.; Fait, J. F.; Freeman, G. K. W.; Thornton, P.; Ironmonger, D. J. *Inorg. Chem.* **1990**, *29*, 1648.
(27) (a) Cotton, F. A.; Poli, R. *Inorg. Chem.* **1987**, *26*, 3310. (b) Cotton, F. A.; Luck, R. L. *Inorg. Chem.* **1989**, *28*, 182.
(28) Boyd, I. W.; Wedd, A. G. *Aust. J. Chem.* **1976**, *29*, 1829.
(29) Minisclоux, C.; Martino, G.; Sajus, L. *Bull. Soc. Chim. Fr.* **1973**, 2179.
(30) Block, E.; Kang, H.; Ofori-Okai, G.; Zubieta, J. *Inorg. Chim. Acta* **1989**, *166*, 155.
(31) Cotton, F. A.; Luck, R. L.; Son, K.-A. *Inorg. Chim. Acta* **1990**, *173*, 131. We are grateful to Prof. Cotton for providing a copy of the manuscript prior to publication.

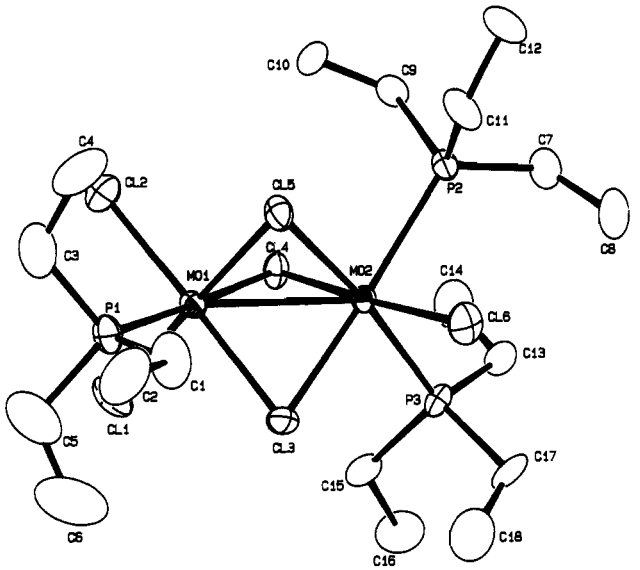

Figure 6. ORTEP view of the $Mo_2Cl_6(PEt_3)_3$ structure with the numbering scheme employed. The ORTEP plot files were modified with the program PLOTMD for label position optimization.[50]

fraction methods. Both molecules have the same geometry, which consists of a confacial bioctahedron with the anti configuration of the terminal ligands (Figures 5 and 6). Neither molecule has imposed crystallographic symmetry, but both have an ideal plane of symmetry, which contains the two molybdenum atoms, the atoms P(1) and Cl(6), and one of the bridging chlorine atoms [Cl(1) for the PMe_2Ph structure, and Cl(4) for the PEt_3 structure]. The structure of the PEt_3 derivative contains an interstitial CH_2Cl_2 molecule.

Relevant structural parameters for the two molecules are compared in Table II. The most notable feature is the difference of the metal–metal bond length, which is ca. 0.1 Å shorter for the PMe_2Ph derivative (2.6582 (5) vs 2.753 (2) Å for the PEt_3 derivative). Mo–Mo bonds in other similar triply chloride-bridged compounds are in the 2.52–2.78 Å range for $Mo_2Cl_9^{3-}$ anions,[32] 2.69–2.76 Å for $Mo_2Cl_7(PMe_3)_2^-$ anions,[27b] 2.815 (4) Å for monoclinic, nonsolvated $Mo_2Cl_6(PEt_3)_3$,[31] 2.746 (9) Å for $Mo_2Cl_7(SMe_2)_2^-$,[26a] and 2.6896 (6) Å for $Mo_2Cl_3(\mu\text{-}Cl)_3(THT)_3$.[26b]

The difference of metal–metal distance between the PEt_3 and PMe_2Ph complexes is in sharp contrast with the practically identical distances to the ligands. Average values for various distances (the first number in each category refers to the PMe_2Ph derivative, the second to the PEt_3 derivative) are as follows: $Mo\text{–}Cl_{b,trans\text{-}to\text{-}P}$, 2.49 (2), 2.49 (1) Å; $Mo\text{–}Cl_{b,trans\text{-}to\text{-}Cl}$, 2.46 (2), 2.45 (2) Å; $Mo\text{–}Cl_t$, 2.371 (4), 2.376 (8) Å; Mo–P, 2.55 (2), 2.56 (2) Å. The different metal–metal distance reflects more on the bond angles at the $Mo(\mu\text{-}Cl)_3Mo$ moiety: Mo–Cl–Mo, 64.8 (1), 67.7 (1)°; Cl–Mo–Cl, 94 (2), 92 (3)°.

As expected, the bonds to the terminal chlorine atoms are shorter than those to the bridging ones. Among the latter, those that are trans to phosphine ligands are significantly longer than those trans to the chloride ligands, in agreement with the known trans influence of these ligands. These parameters compare well with those of the edge-sharing bioctahedral $Mo_2Cl_6(PEt_3)_4$.[11] The only slight discrepancy is found for the $Mo\text{–}Cl_b$ distances, which are slightly longer in the edge-sharing dimer [$Mo\text{–}Cl_{b,trans\text{-}to\text{-}P}$, 2.521 (4) Å; $Mo\text{–}Cl_{b,trans\text{-}to\text{-}Cl}$, 2.480 (4) Å],[11] perhaps reflecting a slight compression on the bonds in the face-sharing dimers because of the stronger metal–metal interaction.

$Mo_2Cl_6(PMe_2Ph)_4$. The only other edge-sharing bioctahedral compound of Mo(III) with monodentate ligands that has been characterized crystallographically is $Mo_2Cl_6(PEt_3)_4$.[11] Mo_2Cl_6-

(32) Stranger, R.; Smith, P. W.; Grey, I. E. *Inorg. Chem.* **1989**, *28*, 1271 and references therein.

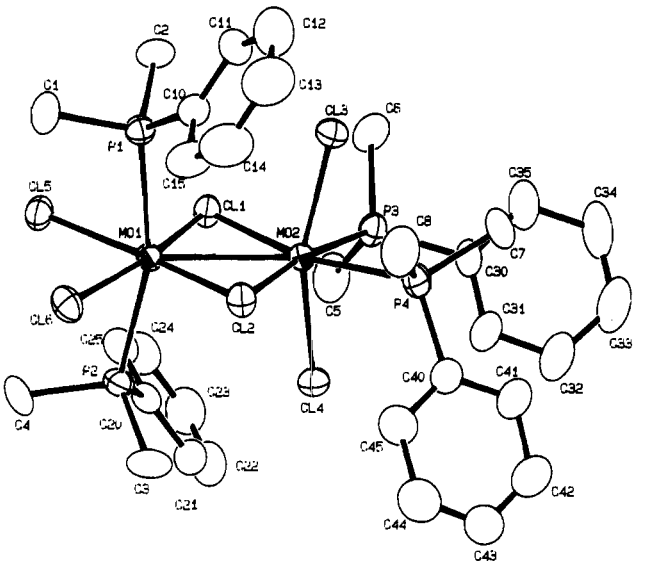

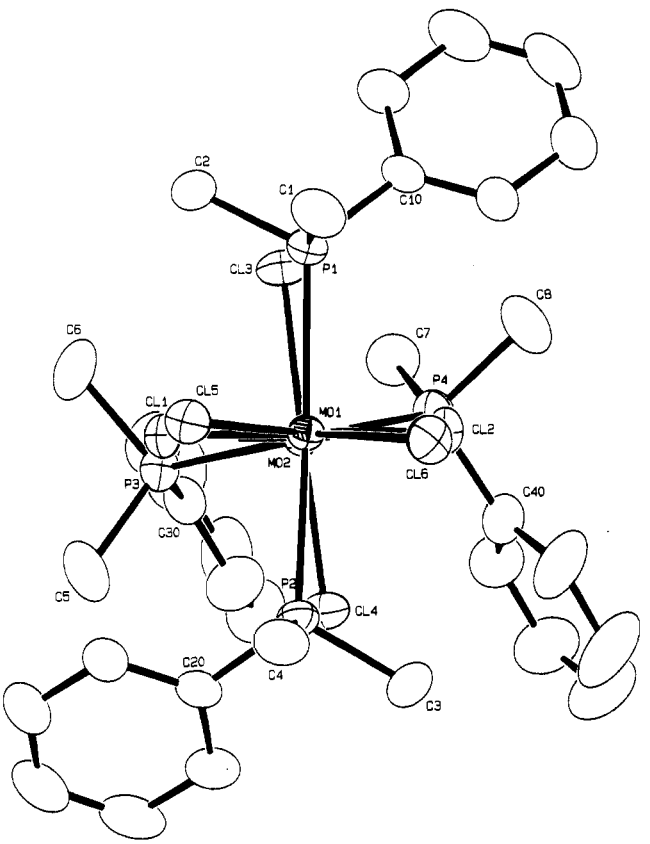

Figure 7. Two ORTEP views of the $Mo_2Cl_6(PMe_2Ph)_4$ structure with the numbering scheme employed. The ORTEP plot files were modified with the program PLOTMD for label position optimization.[50]

$(PMe_2Ph)_4$ crystallizes from $CHCl_3$/heptane with two interstitial chloroform molecules. Two views of the dinuclear molecule are shown in Figure 7. Geometrically, the molecule can be described as a distorted edge-sharing bioctahedron. The axial ligands [P(1) and P(2) on Mo(1) and Cl(3) and Cl(4) on Mo(2)] are bent outward in a way indicative of significant van der Waals repulsive *ax,ax* interactions. This distortion is undoubtedly caused by the strong metal–metal interaction (Mo–Mo: 2.8036 (8) Å) which also induces a distortion in the angular parameters of the Mo_2Cl_2 core [average Cl(1)–Mo–Cl(2) angle = 108.5 (12)°, average Mo(1)–Cl–Mo(2) angle = 71.45 (4)°]. A third distortion is represented by the skewing of one octahedron with respect to the adjacent one and is most evident from the projection along the Mo–Mo vector in Figure 7b. Torsion angles are as follows: Cl(3)–Mo(2)–Mo(1)–P(1), -6.65 (4)°; Cl(4)–Mo(2)–Mo(1)–P-

Scheme I

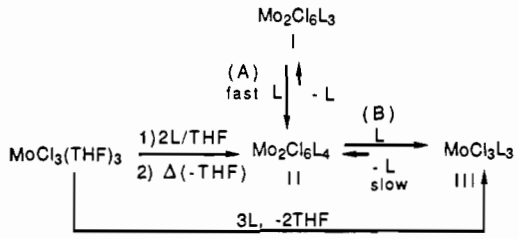

(2), −10.44 (4)°. The geometry at Mo(2) appears more distorted than that at Mo(1) with respect to the bridging ligands, as evidenced by the average deviation from the equatorial least-squares planes: for Cl(1), Cl(2), Cl(5), and Cl(6) (distance of Mo(1) from the plane is 0.014 Å) such average deviation is 0.084 Å, whereas for Cl(1), Cl(2), P(3), and P(4) (distance of Mo(2) from the plane is 0.019 Å) the average deviation is 0.179 Å. This distortion might also be related to the strong metal–metal interaction, although other strongly bound edge-sharing bioctahedral geometries [e.g. $Mo_2X_6(dppe)_2$ (X = Cl, Br),[12b,c] $Mo_2Cl_6(EtSCH_2CH_2SEt)_2$,[12d] and $Mo_2Cl_4(SEt)_2(EtSCH_2CH_2SEt)_2$[12e]] only show steric effects on the axial ligands and on the angles at the $Mo_2(\mu\text{-}X)_2$ core. For the isostructural $Mo_2Cl_6(PEt_3)_4$ compound,[11] the two edge-sharing equatorial planes are perfectly coplanar since they lie on a crystallographic mirror plane. A more likely cause for this distortion is the van der Waals repulsion between the axial chlorine atoms on Mo(2) and the phenyl groups attached to the axial phosphorus atoms on Mo(1). As is evident from the projection in Figure 7b, the axial chlorine atoms have distorted in such a way as to move away from these phenyl rings. Relevant contacts are as follows: Cl(3)···P(1), 3.605 Å; Cl(3)···C(10), 3.527 Å; Cl(4)···P(2), 3.534 Å; Cl(4)···C(20), 3.443 Å. The sum of the van der Waals radii is $r_{Cl} + r_P = 3.70$ Å and $r_{Cl} + r_C$ (half-thickness of an aromatic nucleus) = 3.65 Å.[33] The reciprocity of the steric interaction is shown by the bending of the P–C(phenyl) bond away from the least-squares plane of the corresponding ring. For the phenyl ring attached to P(1), the average deviation of the ring carbon atoms from the plane is 0.004 Å, whereas P(1) is at a 0.080 Å distance. For the phenyl on P(2), these displacements are 0.002 and 0.021 Å, respectively.

The most significant bond distance is the one between the two metal atoms, which is 2.8036 (8) Å. This compares well with that of other chloride-bridged edge-sharing bioctahedral Mo(III) compounds [2.789 (1) Å for $Mo_2Cl_6(dppm)_2$ (type IIa),[12a] 2.762 (1) Å for $Mo_2Cl_6(dppe)_2$ and 2.785 (3) Å for $Mo_2Cl_6(Et_2PCH_2CH_2PPh_2)_2$ (type IIb),[12b] and 2.735 (2) Å for $Mo_2Cl_6(EtSCH_2CH_2SEt)_2$ (type IIc)[12d]], but markedly differs from that of the previously reported $Mo_2Cl_6(PEt_3)_4$ compound [3.730 (1) Å] with the same relative geometry of the coordination sphere. *This is over 0.9-Å difference in the metal–metal bond separation for the simple replacement of PEt_3 with PMe_2Ph!*

The Mo–Cl_b bond length averages are 2.383 (3) Å (trans to chlorides) and 2.418 (2) Å (trans to phosphines). These are shorter than the corresponding distances in the face-sharing dimers discussed above and support the idea of a bond compression resulting from the metal–metal interaction. The Mo–Cl_t distances (average 2.42 (2) Å) are, on the other hand, longer than those found for the above face-sharing bioctahedral compounds and for $Mo_2Cl_6(PEt_3)_4$.[11] The Mo–P distances are in the 2.57–2.60 Å range, which is typical for this distance, but the data do not correlate with known trans-influence trends.

Discussion

The synthetic and reactivity work illustrated in equations 1–8 can be assembled in a single scheme (Scheme I). II is the kinetic product of the thermal THF loss (in refluxing toluene) from a mixture obtained by interacting $MoCl_3(THF)_3$ and the ligand L in a 1:2 ratio in THF.[34a]

The dimer II is thermodynamically unstable toward disproportionation to I and III. Scheme I implies that the disproportionation mechanism involves loss of ligand L to produce the confacial bioctahedral dimer I and that the ligand which is released during this process interacts with more II to generate III. Although this mechanism is not proven by our data, it is consistent with several qualitative observations. Interaction between I and L proceeds rapidly to produce II in a practically quantitative manner. Thus, equilibrium A in Scheme I is substantially shifted toward compound II. Interaction of II with L to produce III proceeds at a much slower rate, which roughly corresponds to the rate of disproportionation. For both phosphine systems, small amounts of free phosphine are observed when the disproportionation of II reaches an equilibrium position. This observation also proves that the interaction between II and L is not a quantitative reaction. However, equilibrium B in Scheme I must be shifted toward III more than equilibrium A is shifted toward II, because the two equilibria combine to give the disproportionation reaction, which is largely shifted toward products I and III. Thus, in a phosphine-rich environment, the stability trend of $MoCl_3$–phosphine adducts is III ≫ II > I.

An equilibrium between mononuclear $MoCl_6^{3-}$ and face-sharing bioctahedral $Mo_2Cl_9^{3-}$ was reported by Lewis et al. No evidence for an edge-sharing bioctahedral $Mo_2Cl_{10}^{4-}$ intermediate was given.[34b] In the related tungsten(III) chemistry, the equilibrium between the edge-sharing and face-sharing $W_2Cl_6(PEt_3)_n$ (n = 3,4) has been described. In that case, the formation of mononuclear derivatives was not observed.[23]

We can now answer a question that was raised in our earlier study.[11] We had observed that $Mo_2Br_6(dppe)_2$ reacts with refluxing THF to regenerate its mononuclear $MoBr_3(dppe)(THF)$ precursor.[12c] In this process, a Mo–Mo bond (2.799 (7) Å) is broken. However, $Mo_2Cl_6(PEt_3)_4$ reacts in THF at room temperature to yield products different than its mononuclear THF adduct precursor(s) (by UV/visible monitoring). As a possible explanation for this behavior, it occurred to us that the same chemistry described in Scheme I might take place in THF. In fact, we have now shown that stirring $Mo_2Cl_6(PEt_3)_4$ in THF at room temperature, followed by removal of the solvent and redissolution in $CDCl_3$, yields an equilibrium mixture containing $MoCl_3(PEt_3)_3$ and $Mo_2Cl_6(PEt_3)_3$ in a 1:1 ratio and corresponding to about 50% conversion of eq 6 with no evidence for the production of THF-containing Mo products. In addition, the interaction of $MoCl_3(THF)_3$ with PEt_3 in a 2:3 ratio *in THF* eventually yielded $Mo_2Cl_6(PEt_3)_3$ selectively. These results prove that loss of PEt_3 from II to produce I is more favorable than takeup of THF to produce $MoCl_3(PEt_3)_2(THF)$ and that a hypothetical $MoCl_3(PEt_3)_2(THF)$ would be unstable with respect to $Mo_2Cl_6(PEt_3)_3$ and $MoCl_3(PEt_3)_3$ in THF. The same behavior is not observed for $Mo_2X_6(dppe)_2$ (X = Cl, Br), possibly because of the ligand chelate effect. The only observed reactivity in that case is the addition of THF to form the mononuclear adduct where the diphosphine chelation has been retained.

It is relevant to observe here that the trend of relative stability for mononuclear vs dinuclear structures when L = phosphine is opposite to what was found when L = THF. The mononuclear $MoCl_3(THF)_3$ complex spontaneously loses THF to sequentially generate II and ultimately I.[24] The effect of the nature of the neutral ligand L on the equilibria illustrated in Scheme I is one of the interesting aspects of the chemistry described in this work. Another interesting aspect is the effect of the ligand L on the extent of metal–metal bonding in the dinuclear species I and II. We shall now address the effect on the metal–metal interaction, and we shall come back to the effect on the monomer/dimer equilibria later.

(33) Weast, R. C., Ed. *Handbook of Chemistry and Physics*, 57th ed.; CRC Press: Cleveland, OH, 1976.

(34) (a) This solution is probably a 1:1 mixture of $MoCl_3(THF)_2(PR_3)$ and $MoCl_3(PR_3)_3$. ^1H NMR monitoring of $MoCl_3(THF)_3 + 3PR_3$ reactions (PR_3 = PEt_3, PMe_2Ph) reveals a kinetic trans effect. *mer-trans*-$MoCl_3(THF)_2(PR_3)$ is generated in a first fast step which is followed by the slow transformation to the $MoCl_3(PR_3)_3$ final product. A full account of these findings will be published separately. (b) Lewis, J.; Nyholm, R. S.; Smith, P. W. *J. Chem. Soc. A* **1969**, 58.

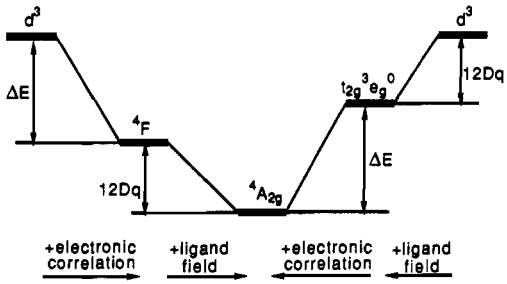

Figure 8. Electronic ground state for an octahedral d^3 ion and its relationship to the monoelectronic d^3 configuration, to the ground spectroscopic term (^4F) for an isolated d^3 atom, and to the ground state configuration (t_{2g}^3) in the strong field limit. The possible effect of spin–orbit coupling has not been considered.

Metal–Metal Bond Formation in the Dinuclear Compounds. (a) Edge-Sharing Bioctahedral Systems. While all the edge-sharing bioctahedral Mo(III) compounds containing bidentate ligands (type IIa–c) are known to be strongly metal–metal bonded (Mo–Mo = 2.5–2.8 Å)[12f] and almost diamagnetic, we have recently found that the use of the monodentate PEt_3 ligand results in the formation of a compound of type IId, the first edge-sharing bioctahedral derivative of Mo(III) that does not contain a metal–metal interaction (Mo–Mo = 3.730 (1) Å).[11] Since several factors vary on going from the Mo–Mo-bonded structures to the nonbonded one (relative disposition, denticity, steric, and electronic properties of the ligands), we decided to probe the effect of each of these factors and started with the use of the monodentate phosphine PMe_2Ph.

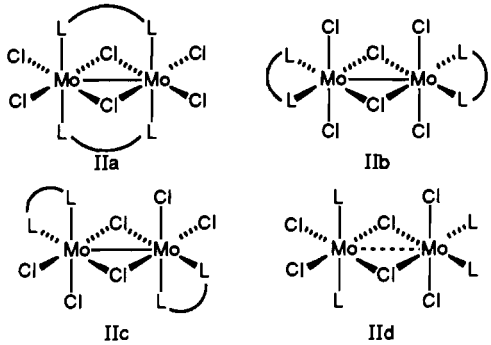

The formation of the metal–metal-bonded complex $Mo_2Cl_6(PMe_2Ph)_4$ of type IId demonstrates that the electronic properties of the phosphine ligand are a decisive factor in the control of the metal–metal bond formation. The two phosphines have not too dissimilar cone angles (PEt_3, 132°; PMe_2Ph, 122°).[35]

We shall now discuss the possible ways in which the electronic properties of the phosphine ligand affect the ability of the two metals to interact with each other. The problem can be represented by equilibrium 9. Obviously, competing driving forces, some

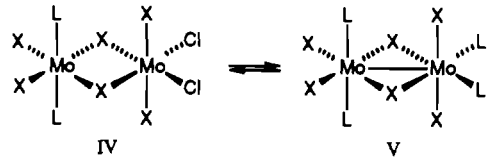

(9)

favoring the non-metal–metal-bonded isomer IV and others favoring the metal–metal-bonded isomer V, must be at work. A driving force for the formation of the metal–metal-bonded isomer is clearly the interaction between the two metals to form the direct bond. The nature of this metal–metal interaction has been extensively discussed.[36] Our semiempirical MO calculations by the Fenske–Hall method on the $Mo_2Cl_6(PH_3)_4$ model system (vide infra) indicate a metal–metal interaction of type $\sigma^2\pi^2\delta^{*2}$ in good qualitative agreement with those carried out[12e] by the same method for $Mo_2Cl_4(\mu\text{-}SH)_2(SH_2)_4$ and with the extended Huckel calculations for Re_2Cl_{10}.[36a]

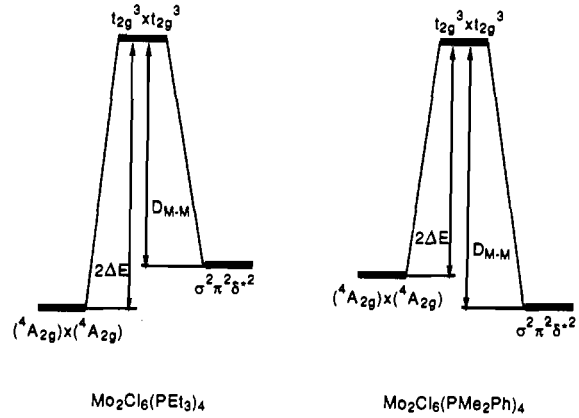

Figure 9. Relative energy of the ground states for the metal–metal-bonded and -nonbonded isomers of structure IId.

The competing stabilization of isomer IV must be the inherent stability of the t_{2g}^3 electronic configuration in a mononuclear octahedral environment, which is mainly an electronic correlation effect. Figure 8 shows the energetics of the $^4A_{2g}$ ground state for a d^3 ion in an octahedral ligand field (we approximate the symmetry of the mononuclear system as ideally octahedral for the sake of simplicity). The left-hand side of Figure 8 shows how to obtain the ground state from the atomic d^3 configuration by successive application of the electronic correlation and the ligand field as perturbation effects. The separation ΔE is a function of the Slater–Condon–Shortley integrals F_0, F_2, and F_4,[37] (or the related Racah parameters B and C). The alternative approach of reversing the order of perturbation on the monoelectronic Hamiltonian is shown on the right hand side of the same figure. The stabilization of the ground state with respect to the monoelectronic ($t_{2g}^3e_g^0$) configuration is again ΔE. Thus, the stability of the ground state depends on two factors: electronic correlation and ligand field strength. The approximation is made of neglecting spin–orbit coupling effects.

The t_{2g}^3 configuration is also the starting point for our mental construction, by the use of the LCAO-MO method, of the metal–metal bond formation. In Figure 9, we compare the stabilization of two mononuclear octahedral Mo(III) units at a distance that precludes any direct metal–metal bond formation (isomer IV of equilibrium 9), with a metal–metal-bonded Mo_2 core (isomer V). We labeled $D_{M\text{-}M}$ the energy difference between the metal–metal-bonded system and the ideal monoelectronic t_{2g}^3 system. This number is not quite a Mo–Mo bond disruption energy in the usual sense since, upon breaking the bond, two systems in the $^4A_{2g}$ state will arise. $D_{Mo\text{-}Mo}$ as defined in Figure 9 is rather a measure of the intrinsic strength of the metal–metal bond.

Given the common starting point (the t_{2g}^3 configuration) where ligand field effects have already been considered, the relative stability of the metal–metal-bonded and -nonbonded isomers is not expected to depend on ligand field effects. This argument can be better seen by going back to the most popular interpretation of the ligand field effects: orbitals having the maximum density away from the ligands will be stabilized, whereas those with maximum density in the regions occupied by the ligands will be destabilized. In the metal–metal-bonded isomer, the three orbitals occupied by the six metal electrons (σ, π, and δ^*) all have maximum density away from the ligands and will experience a stabilizing effect to a first approximation identical with that operating on two separate t_{2g} sets in mononuclear octahedral environments.

Thus, to the level of approximation used in the present discussion, the relative stability of the metal–metal-bonded and

(35) Tolman, C. A. *Chem. Rev.* **1977**, *77*, 313.
(36) (a) Shaik, S.; Hoffmann, R.; Fisel, C. R.; Summerville, R. H. *J. Am. Chem. Soc.* **1980**, *102*, 4555. (b) Anderson, L. B.; Cotton, F. A.; DeMarco, D.; Fang, A.; Ilsley, W. H.; Kolthammer, W. S.; Walton, R. A. *J. Am. Chem. Soc.* **1981**, *103*, 5078. See also ref 12a and 12e.
(37) Condon, E. U.; Shortley, G. H. *The Theory of Atomic Spectra*; Cambridge University Press: Cambridge, England, 1935.

-nonbonded isomers is only a function of the electronic correlation effects and the strength of the metal–metal interaction. The ground states for the two different isomers do not correlate with each other. In D_{2h} symmetry, the ground state for the nonbonded isomer (left-hand side of either diagram in Figure 9) is predicted to split into four states, $^1B_{1u}$, $^3B_{1u}$, $^5B_{1u}$, and $^7B_{1u}$, by the antiferromagnetic spin exchange Hamiltonian, the first of which has the lowest energy, whereas the ground state for the metal–metal-bonded isomer is of ^1A_g type. Thus, each isomer is expected to lie on a potential energy minimum. The question arises as to whether the *same* molecule could be found to exist in either isomeric form, that is metal–metal bonded and nonbonded. If this were possible, the case could be described as a sui generis example of "bond stretch" isomerism.[38] There are, to the best of our knowledge, no examples of this kind of isomerism for bonds, either single or multiple, connecting two transition elements, nor are there examples for homonuclear covalent bonds of any element. A bond stretch isomerism has been computed for the bridgehead silicon–silicon bond of bicyclo[1.1.0]tetrasylane.[39] We have found no evidence in this study for a metal–metal-bonded $Mo_2Cl_6(PEt_3)_4$ isomer or a metal–metal-nonbonded $Mo_2Cl_6(PMe_2Ph)_4$ isomer, but we cannot exclude that for each system a small amount of the second isomer is present in a fast thermal equilibrium on the NMR time scale.

For $Mo_2Cl_6(PEt_3)_4$, which is found to exist as a nonbonded isomer in the solid state,[11] the observed temperature-dependent ^1H NMR shifts (Figure 3a) indicate that there is no appreciable deviation from Curie behavior over the range investigated. Therefore, the critical temperature must be much lower than the minimum temperature attained in the ^1H NMR experiment, and the value of the antiferromagnetic coupling constant, J, must be small. For $Mo_2Cl_6(PMe_2Ph)_4$, which exists as the metal–metal-bonded isomer in the solid state, the increase of the ^1H NMR paramagnetic shifts at higher temperature could be due to either an increased population of the paramagnetic $\sigma^2\pi^2\delta^{*1}\delta^1$ excited state or to an increased population of the higher energy nonbonded isomer through a fast equilibrium on the NMR time scale or to a combination of both effects.

The question that now must be addressed is: What is the effect of the ligands (specifically, the phosphine ligands) on the electron correlation effects and on the intrinsic strength of the metal–metal interaction? The effect of the ligands on the extent of correlation effects are usually described[40] in terms of the nephelauxetic (or cloud expansion) phenomenon, which is a result of the partial delocalization of metal electron density onto the ligands. A higher effect results in a diminished electronic correlation and a higher stability (lower energy) for the high-spin ground state. It is generally thought that the effect is directly related to the ability of the ligand system to delocalize electron density through π interactions. This is because the t_{2g} set of atomic orbitals where the electrons reside do not have the right symmetry to engage in σ interactions with the ligands. Along this line of reasoning, it would be logical to expect a greater stabilization of the high-spin structure in the case of PMe_2Ph, since this phosphine should display a greater π-accepting ability.[41] However, the PMe_2Ph structure is the one where the metal–metal-bonded isomer is more favored. A cloud expansion effect might also be the indirect result of a greater σ donation, since this would tend to increase the electron density at the metal and consequently the size of all the orbitals because of increased shielding of the nuclear charge. This explanation would better fit the data since PEt_3 is a better σ donor than PMe_2Ph.[35,42] There are few studies of the nephelauxetic effect of phosphine ligands. The investigation of the electronic absorption spectra of $PtCl_3L^-$ complexes places PEt_3 lower than PPh_3 in the nephelauxetic series.[43] However, Pt(II) is a much better π base than Mo(III), giving rise to metal–phosphorus bonds with a greater component of π back-donation. Conclusions about the relative nephelauxetic effect of different ligands that are valid for Pt(II) are not necessarily valid for Mo(III).

The other way a ligand might affect the position of equilibrium 9 is through a direct influence on the intrinsic strength of the metal–metal interaction. This point is also difficult to address since a measure of the metal–metal bond disruption energy (conceptually possible, although experimentally difficult) would give a measure of the $(D_{Mo-Mo} - 2\Delta E)$ difference as defined in Figure 9. We can attempt to make some considerations based on the results of our Fenske–Hall MO calculations. The contribution of phosphorus atomic orbitals to the σ, π, and δ^* orbitals that accommodate the six metal d electrons is negligible (<1%). These MO's are mainly made up of molybdenum orbitals and chlorine (both bridging and terminal) lone pairs. We conclude that the nature of the halide ligands might have a direct effect on the intrinsic metal–metal bond strength, whereas the nature of the neutral ligands (when they do not contain potentially π-donating lone pairs) probably does not.

The basicity of the ligand could influence the strength of the metal–metal interaction in an indirect way. As discussed earlier in relation to the nephelauxetic effect, the more basic ligand is expected to expand all metal orbitals. Therefore, a better overlap might result, giving rise to a stronger metal–metal interaction. However, PEt_3 is certainly the more basic among the two phosphines investigated here and would be expected to give rise to a stronger metal–metal interaction based on the above consideration, although in fact it has the opposite effect. Thus, the nature of the phosphine ligand does not seem to greatly affect the intrinsic strength of the metal–metal interaction.

In conclusion, it seems that the position of equilibrium 9 is the result of a delicate balance between the stability of the high-spin configuration obtained from the nonbonding interaction of two octahedral t_{2g}^3 systems and that which is gained by the formation of the metal–metal $\sigma^2\pi^2\delta^{*2}$ interaction. The effect of the nature of the phosphine on this equilibrium is dramatic, and seems to be mainly related to electronic correlation effects. However, it is to be emphasized that the above discussion is based on very qualitative argumentations and makes use of several approximations. Furthermore, experimental data on the nephelauxetic effect of phosphine ligands are not available for octahedral complexes of early transition metals. A more detailed investigation of this and other related systems is necessary before a full understanding of this phenomenon can be achieved.

It seems appropriate at this point to mention the long-standing puzzling discrepancy between the structure of $Re_2Cl_6(dppe)_2$, which is of type IIb with a long metal–metal separation (3.809 (1) Å),[44] and those of other rhenium(III) dimers of type IIa, which show strong metal–metal interactions.[45] There is, so far, no clear explanation for this difference although hypotheses based on the involvement of steric interactions have been advanced.[12f] We suggest that the rhenium system experiences effects similar to the molybdenum system reported here. For rhenium(III), the d^4 configuration gives rise to a $^3T_{1g}$ ground state in a strong octahedral field, formally derived from the $t_{2g}^4e_g^0$ monoelectronic configuration. On the other hand, two such metal centers in close proximity can give rise to a $\sigma^2\pi^2\delta^{*2}\delta^2$ metal–metal interaction of order 2. A slight change of the electronic nature of the phosphine ligand, and not necessarily of its steric requirements, might tip

(38) Jean, Y.; Lledos, A.; Burdett, J. K.; Hoffmann, R. *J. Am. Chem. Soc.* **1988**, *110*, 4506.
(39) (a) Dabisch, T.; Schöller, W. W. *J. Chem. Soc., Chem. Commun.* **1986**, 896. (b) Schöller, W. W.; Dabisch, T.; Busch, T. *Inorg. Chem.* **1987**, *26*, 4383. (c) von Raguć Schleyer, P.; Sax, A. F.; Kalcher, J.; Janoschek, R. *Angew. Chem., Int. Ed. Engl.* **1987**, *26*, 364. (d) Boatz, J. A.; Gordon, M. S. *J. Phys. Chem.* **1989**, *93*, 2888.
(40) (a) Schäffer, C. E.; Jørgensen, C. K. *J. Inorg. Nucl. Chem.* **1958**, *8*, 143. (b) Ballhausen, C. J. *Introduction to Ligand Field Theory*; McGraw-Hill: New York, 1962. (c) Huheey, J. E. *Inorganic Chemistry*, 4th ed.; Harper & Row: New York, 1983.
(41) Atwood, J. D. *Inorganic and Organometallic Reaction Mechanisms*; Brooks/Cole: Monterey, CA; 1985; pp 103–106 and references therein.
(42) Rahman, M. M.; Liu, H.-Y.; Eriks, K.; Prock, A.; Giering, W. P. *Organometallics* **1989**, *8*, 1.
(43) Chang, T.-H.; Zink, J. I. *Inorg. Chem.* **1986**, *25*, 2736.
(44) Jaeker, J. A.; Robinson, W. R.; Walton, R. A. *J. Chem. Soc., Dalton Trans.* **1975**, 698.
(45) Barder, T. J.; Cotton, F. A.; Lewis, D.; Schwotzer, W.; Tetrick, S. M.; Walton, R. A. *J. Am. Chem. Soc.* **1984**, *106*, 2882.

the balance in favor of either isomer. Certainly, there does not appear to be a drastic difference in steric effects in the two molybdenum systems reported here.

(b) Face-Sharing Bioctahedral Systems. Turning now to the confacial bioctahedral compounds, the first obvious observation to make is that for both phosphine systems (PMe_2Ph and PEt_3) a metal–metal-bonded structure is obtained. This may be at least in part due to the fact that, in the complete absence of metal–metal interactions or distortions of any other kind, a confacial bioctahedral structure tends to place the two metal centers closer to each other with respect to an edge-sharing bioctahedral structure with the same bridging ligands.[46] The PEt_3 system, however, exhibits a significantly longer metal–metal separation, ca. 0.1 Å longer than the same parameter in the PMe_2Ph structure. This observation seems to suggest that factors analogous to those operating on the edge-sharing system discussed above are also operating on the face-sharing structure. A word of caution is necessary here. Although 0.1-Å difference is certainly much greater than the experimental error on the individual lengths, the very delicate balance of internal forces may render the metal–metal distance quite susceptible to external forces, such as packing forces in the crystalline state and van der Waals and dipole–dipole interactions in solution. In fact, the crystal structure of $Mo_2Cl_6(PEt_3)_3$ in a different crystal system (obtained from toluene/hexane) has recently been obtained and shows a Mo–Mo separation of 2.815 (4) Å,[31] that is, ca. 0.06 Å longer than the one reported here for the same compound obtained from CH_2Cl_2/heptane. However, we observe that the ^1H NMR spectra for the two phosphine systems dissolved in the same solvent show slightly greater paramagnetic shifts for the α-protons of the compound with the PEt_3 ligand, in apparent agreement with a weaker metal–metal interaction for this compound.

Figure 9 will also hold for the confacial bioctahedral system upon proper change of the symmetry labels (the electronic configuration of the metal–metal bond in face-sharing bioctahedral d^3–d^3 systems is[47] $\sigma^2\pi^4$). The same arguments presented above for the edge-sharing bioctahedral system can be employed here to show that the nature of the phosphine ligand probably does not influence directly the intrinsic strength of the metal–metal interaction (there is no significant phosphorus contribution in the metal–metal-bonding MO's). There is, to date, no metal–metal-nonbonded isomer for a Mo(III) face-sharing bioctahedral structure and an interesting question is whether any such compound could be isolated in this isomeric form.

Magnetic Properties vs Metal–Metal Bonding. For both face-sharing $Mo_2Cl_6L_3$ compounds (L = PMe_2Ph, PEt_3) and for the edge-sharing bioctahedral $Mo_2Cl_6(PMe_2Ph)_4$, the temperature-dependent ^1H NMR spectra are consistent with a diamagnetic ground state and a slightly populated paramagnetic excited state. A comparison of the two structural types with the same phosphine ligand shows that the paramagnetic shifts are greater in the face-sharing compound, although this has the shorter Mo–Mo distance and therefore, presumably, the stronger metal–metal interaction. In fact, metal–metal bonding is of the $\sigma^2\pi^4$ type in the face-sharing compounds and of the $\sigma^2\pi^2\delta^{*2}$ type in the edge-sharing compounds. This apparent contradiction is reconciled when comparing the results of the Fenske–Hall MO calculations on the model $Mo_2Cl_6(PH_3)_n$ (n = 3, 4) systems (Figure 10).

For the edge-sharing structure, the raising of the δ orbital above the δ^* orbital is due to the interaction of the bridging chlorine lone pairs as discussed in the literature.[36] When the metal–metal separation is increased from 2.70 to 3.00 Å, the energy of the δ orbital increases and that of the π^* orbital decreases so that the LUMO is the former at M–M < ca. 2.9 Å and the latter at higher distances. On the other hand, the energy of the HOMO remains approximately unaltered. The result of this trend is that the

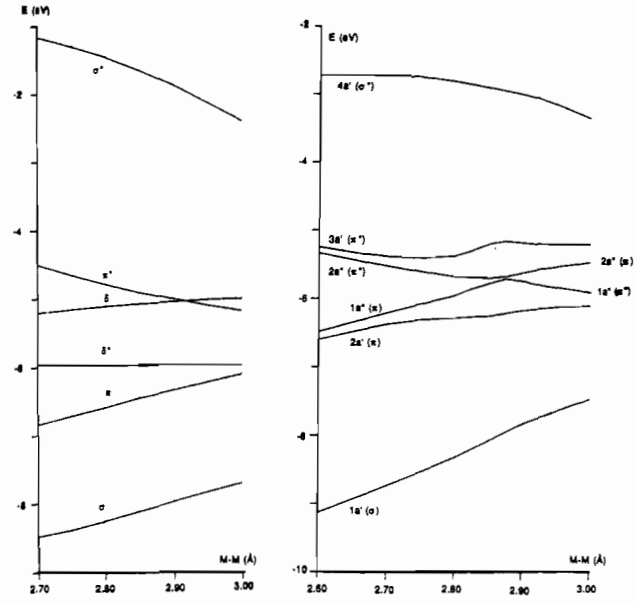

Figure 10. Frontier orbital region for (a) $Mo_2Cl_6(PH_3)_4$ of structure IId and (b) $Mo_2Cl_6(PH_3)_3$ of structure Ia, as a function of the metal–metal separation.

HOMO–LUMO gap (ca. 0.8 eV) is not drastically affected by a change in metal–metal bond distance in the range illustrated.

On the other hand, the face-sharing bioctahedral structure shows a HOMO–LUMO gap that markedly depends on the metal–metal separation and is smaller, in the range of Mo–Mo distances observed for the $Mo_2Cl_6L_3$ compounds, than for the corresponding edge-sharing structure, in perfect agreement with the experimental ^1H NMR data. For our model compound, both the e' (π, HOMO) and e'' (π^*, LUMO) combinations in D_{3h} symmetry are split (a' + a'') because of the low symmetry (C_s) of the molecule. Since each of these pairs are bases for the same irreducible representation of the symmetry group, the lines in Figure 10b cannot cross as they do[47d] for the D_{3h} $Mo_2Cl_9^{3-}$ and smoothly change character from bonding to antibonding or vice versa on going from one side to the other of the diagram, passing through a situation of essentially nonbonding character.

Monomer/Dimer Equilibria. Equilibrium 10 is shifted to either side depending on the nature of L. For L = phosphine, the mononuclear product on the right hand side is favored whereas for L = THF the system evolves to quantitatively form the face-sharing dimer.[24] Thus, the reaction enthalpy for reaction 10 must be negative when L = phosphine because the presumably negative reaction entropy does not impede the reaction to proceed toward the right. On the other hand, a less negative or a positive ΔH must be obtained for L = THF.

$$Mo_2Cl_6L_3 + 3L \rightleftharpoons 2MoCl_3L_3 \qquad (10)$$

The main driving force for the formation of $Mo_2Cl_6L_3$ is the formation of the metal–metal interaction. On the other hand, the two monomers on the right-hand side are mainly stabilized by electronic correlation effects in an analogy to the edge-sharing bioctahedral dimers without metal–metal interaction discussed above. In addition, three additional Mo–L bonds are formed on going from the face-sharing dimer to the two mononuclear molecules and these will contribute to the driving force for the forward reaction. The additional contribution of six Mo–(μ-Cl) bonds of the dimer turning into three terminal Mo–Cl bonds is anticipated to slightly favor the dinuclear system but this last contribution does not depend, to a first approximation, on the nature of L. In addition to all these effects, there is an additional complication in that the coordination sphere around the metal center is different in the mononuclear and dinuclear compounds, causing a different stabilization due to ligand field effects.

Therefore, the nature of L affects the position of equilibrium 10 in a manner similar to how it affects equilibrium 9, with the additional factors of the Mo–L bond strength and the different

(46) Cotton, F. A.; Ucko, D. A. *Inorg. Chim. Acta* **1972**, *6*, 161.
(47) (a) Saillant, R.; Wentworth, R. A. D. *J. Am. Chem. Soc.* **1969**, *91*, 2174. (b) Templeton, J. L.; Jacobsen, R. A.; McCarley, R. E. *Inorg. Chem.* **1977**, *16*, 3320. (c) Templeton, J. L.; Dorman, W. C.; Clardy, J. E.; McCarley, R. E. *Inorg. Chem.* **1978**, *17*, 1263. (d) Summerville, R. H.; Hoffmann, R. *J. Am. Chem. Soc.* **1979**, *101*, 3821.

ligand field. Ligands L that form the stronger bonds with the metal will shift the equilibrium toward the monomer. No thermochemical data are available to assess the relative strength of Mo–phosphine and Mo–ether bonds, but we recently argued,[48] on the basis of a qualitative use of Drago's E/C empirical treatment of acid/base interactions,[49] that phosphine ligands should always bind more strongly than ethers, no matter what the nature of the Lewis acid. Thus, this factor alone serves to explain the preference of mononuclear compounds for L = phosphine over THF. Concerning crystal field effects, it is known that phosphines are stronger field ligands than ethers.[40c] Since the number of L ligands increases on going from dimer to monomer, it is expected that crystal field effects will contribute to the relative stabilization of the mononuclear structure in a larger extent when L = phosphine. Thus, this effect also contributes to the observed higher stability of the mononuclear system for L = phosphine.

The effect of L on the stabilization of the quartet ground state of the mononuclear compounds (electronic correlation energy) cannot be assessed because the nephelauxetic effect of phosphine ligands is not known with respect to that of ethers. Concerning the direct effect on the metal–metal bond strength, since the oxygen donor ligand THF has π-type lone pairs, it is expected that it will contribute to the rehybridization of the metal orbitals that are involved in metal–metal bonding in such a way that the overlap of both the σ and the π/δ combination will be increased, as argued by Hoffmann.[47d] Therefore, THF is expected to increase the strength of the Mo–Mo interaction with respect to the phosphines. This effect is also in agreement with the observed trend of reactivity.

Summary and Conclusions

This investigation has shown that the relative stability of monomers and dimers for octahedrally coordinated Mo^{3+} are the result of a delicate balance between metal–metal bond strength, metal–ligand bond strength, ligand field strength, and electronic correlation effects. The latter play a decisive role in the choice between a metal–metal-bonded or a -nonbonded isomer for the edge-sharing bioctahedral complexes. An unprecedented change of over 0.9 Å in the metal–metal distance by the mere substitution of PEt_3 with PMe_2Ph has been observed for this class of compounds.

Several novel observations were made possible by the awareness that octahedrally coordinated $S = {}^3/_2$ Mo(III) systems display relatively sharp ^1H NMR spectra for a structural analysis in solution to be carried out. To date, the study of the structure and reactivity of the octahedral Mo(III) system was largely confined to the isolation of crystalline materials and their investigation by elemental analysis, magnetic susceptibility, and (when single crystals could be obtained) X-ray diffraction. We have reported here that octahedral MoX_3L_3 (L = PMe_3, PMe_2Ph, PEt_3) systems are exclusively meridional in solution, that edge-sharing bioctahedral $Mo_2Cl_6L_4$ (L = PMe_2Ph, PEt_3) compounds maintain in solution their solid-state structure, and that face-sharing bioctahedral $Mo_2Cl_6L_3$ (L = PMe_2Ph, PEt_3) exist in solution as equilibrium mixtures of anti and gauche isomers. We have shown that edge-sharing bioctahedral $Mo_2Cl_6L_4$ compounds are unstable toward disproportionation to mononuclear ($MoCl_3L_3$) and face-sharing bioctahedral ($Mo_2Cl_6L_3$) compounds when L = phosphine. In addition, we have shown that the magnetic properties of metal–metal-bonded dimers with partial population of paramagnetic excited states do not necessarily correlate with the strength of the metal–metal interaction for different structural types. Finally, it was by the application of the ^1H NMR technique that we discovered the tremendous difference in magnetic properties (through the paramagnetic shifts) between the $Mo_2Cl_6L_4$ (L = PEt_3, PMe_2Ph) compounds.

Future investigations will be directed toward seeking a better understanding of the ligand influence on the stability and structure of octahedrally coordinated Mo(III) complexes.

Acknowledgment. Support from the University of Maryland at College Park (UMCP) Department of Chemistry and Biochemistry, the UMCP General Research Board, the Camille and Henry Dreyfus Foundation (through a Distinguished New Faculty Award to R.P.), and the donors of the Petroleum Research Fund, administered by the American Chemical Society, is gratefully acknowledged. The X-ray diffractometer and MicroVax computer system were purchased in part with NSF funds (Grant CHE-84-02155). We thank Dr. Lee Daniels for the collection of X-ray intensity data on the $Mo_2Cl_6(PMe_2Ph)_4 \cdot 2CHCl_3$ compound. H.D.M. is grateful to the UMCP Office of Undergraduate Studies for a Senior Summer Scholarship.

Supplementary Material Available: For compounds $Mo_2Cl_6(PMe_2Ph)_3$, $Mo_2Cl_6(PEt_3)_3 \cdot CH_2Cl_2$, and $Mo_2Cl_6(PMe_2Ph)_4 \cdot 2CHCl_3$, full tables of crystal data, atomic coordinates and isotropic thermal parameters, hydrogen atom parameters, bond distances, bond angles, and anisotropic thermal parameters (33 pages); listings of observed and calculated structure factors (117 pages). Ordering information is given on any current masthead page.

(48) Poli, R.; Walker, J. D. *Inorg. Chem.* **1990**, *29*, 756.
(49) (a) Drago, R. S.; Wayland, B. B. *J. Am. Chem. Soc.* **1965**, *87*, 3571. (b) Drago, R. S. *Struct. Bonding (Berlin)* **1973**, *15*, 73. (c) Drago, R. S.; Parr, L. B.; Chamberlain, C. S. *J. Am. Chem. Soc.* **1977**, *99*, 3203. (d) Drago, R. S.; Wong, N.; Bilgrien, C.; Vogel, G. C. *Inorg. Chem.* **1987**, *26*, 9.
(50) Luo, J.; Ammon, H.; Gilliland, G. L. *J. Appl. Crystallogr.* **1989**, *22*, 186.